Unraveling the Mechanism of Extreme (More than 30 Sigma) Precipitation during August 2018 and 2019 over Kerala, India

PARTHASARATHI MUKHOPADHYAY,[a] PETER BECHTOLD,[b] YUEJIAN ZHU,[c] R. PHANI MURALI KRISHNA,[a] SIDDHARTH KUMAR,[a] MALAY GANAI,[a] SNEHLATA TIRKEY,[a] TANMOY GOSWAMI,[a] M. MAHAKUR,[a] MEDHA DESHPANDE,[a] V. S. PRASAD,[d] C. J. JOHNY,[e] ASHIM MITRA,[e] RAGHAVENDRA ASHRIT,[d] ABHIJIT SARKAR,[d] SAHADAT SARKAR,[a] KUMAR ROY,[a] ELPHIN ANDREWS,[e] RADHIKA KANASE,[a] SHILPA MALVIYA,[a] S. ABHILASH,[f] MANOJ DOMKAWALE,[a] S. D. PAWAR,[a] ASHU MAMGAIN,[d] V. R. DURAI,[e] RAVI S. NANJUNDIAH,[a,g,h] ASHIS K. MITRA,[d] E. N. RAJAGOPAL,[d] M. MOHAPATRA,[e] AND M. RAJEEVAN[i]

[a] *Indian Institute of Tropical Meteorology, Ministry of Earth Sciences, Pune, India*
[b] *European Centre for Medium-Range Weather Forecasts, Reading, United Kingdom*
[c] *Environmental Modeling Center, NOAA/NWS/NCEP, College Park, Maryland*
[d] *National Centre for Medium Range Weather Forecasting, Ministry of Earth Sciences, Noida, India*
[e] *India Meteorological Department, Ministry of Earth Sciences, New Delhi, India*
[f] *Cochin University of Science and Technology, Cochin, India*
[g] *Centre for Atmospheric and Oceanic Sciences, Indian Institute of Science, Bengaluru, India*
[h] *Divecha Centre for Climate Change, Indian Institute of Science, Bengaluru, India*
[i] *Ministry of Earth Sciences, Prithvi Bhawan, New Delhi, India*

(Manuscript received 16 September 2020, in final form 19 February 2021)

ABSTRACT: During August 2018 and 2019 the southern state of India, Kerala, received unprecedented heavy rainfall, which led to widespread flooding. We aim to characterize the convective nature of these events and the large-scale atmospheric forcing, while exploring their predictability by three state-of-the-art global prediction systems: the National Centers for Environmental Prediction (NCEP)-based India Meteorological Department (IMD) operational Global Forecast System (GFS), the European Centre for Medium-Range Weather Forecasts (ECMWF) Integrated Forecast System (IFS), and the Unified Model–based NCUM being run at the National Centre for Medium Range Weather Forecasting (NCMRWF). Satellite, radar, and lightning observations suggest that these rain events were dominated by cumulus congestus and shallow convection with strong zonal flow leading to orographically enhanced rainfall over the Ghats mountain range; sporadic deep convection was also present during the 2019 event. A moisture budget analyses using the fifth major global reanalysis produced by ECMWF (ERA5) and forecast output revealed significantly increased moisture convergence below 800 hPa during the main rain events compared to August climatology. The total column-integrated precipitable water tendency, however, is found to be small throughout the month of August, indicating a balance between moisture convergence and drying by precipitation. By applying a Rossby wave filter to the rainfall anomalies it is shown that the large-scale moisture convergence is associated with westward-propagating barotropic Rossby waves over Kerala, leading to increased predictability of these events, especially for 2019. Evaluation of the deterministic and ensemble rainfall predictions revealed systematic rainfall differences over the Ghats mountains and the coastline. The ensemble predictions were more skillful than the deterministic forecasts, as they were able to predict rainfall anomalies (greater than three standard deviations from climatology) beyond day 5 for August 2019 and up to day 3 for 2018.

SIGNIFICANCE STATEMENT: The purpose of this study is to understand and unravel the large-scale mechanism behind the unprecedented heavy rainfall over Kerala, India, during August 2018 and 2019. The study brings out the importance of probabilistic rainfall predictions for extreme heavy rainfall events. The study reveals that large-scale moisture convergence plays a significant role in the extreme rain of August 2018 and 2019. The extreme rainfall of August is associated with a westward-propagating barotropic Rossby wave. The study also demonstrates that ensemble forecasts of extreme rain by the state-of-the-art prediction systems of GFS, IFS, and NCUM are skillful for longer lead times compared to deterministic models and, therefore, can provide better early warnings to the society.

KEYWORDS: Ensembles; Forecasting; Operational forecasting; Probability forecasts/models/distribution; Short-range prediction

1. Introduction

Heavy rain during the summer monsoon season of June–July–August–September (JJAS) in the windward side of the Western Ghats over the western coast of India along the coastal state of Kerala is not uncommon. The climatological seasonal mean total rainfall of Kerala is 2039.7 mm during JJAS. It is also known that numerical models struggle in capturing the

Supplemental information related to this paper is available at the Journals Online website: https://doi.org/10.1175/WAF-D-20-0162.s1.

Corresponding author: Parthasarathi Mukhopadhyay, mpartha@tropmet.res.in; parthasarathi64@gmail.com

DOI: 10.1175/WAF-D-20-0162.1

orographically induced rain along the western side of the Ghat mountains, mainly due to limitations in resolving the mountains (Mishra et al. 2018; Shashikanth et al. 2014). There are many studies on the orographic rainfall over different regions of the globe (Rotunno and Houze 2007; Shige and Kummerow 2016). However, studies evaluating the model forecast skills for extreme rains over Kerala are rather limited. Earlier studies based on the observations have highlighted the heavy rainfall and cloud pattern over the west coast region of India (Utsav et al. 2017; Kumar et al. 2014; Maheskumar et al. 2014). These suggested that the rainfall over the Kerala state to the west of the Western Ghats mountains occurs mainly from warm clouds and the convection is not deep (confined within 500 hPa or 6 km). Although the state of Kerala receives heavy rain during the southwest monsoon season and shows high variability, the rainfall during August of 2018 and 2019 (particularly during 6–19 August) has exceeded the daily climatology by around 236% and 219%, respectively (Figs. 1a,b). As a result, it caused an unprecedented flooding and devastation over the state with immense loss of precious human lives and properties. The flooding associated with the extreme rain is reported to be the worst in the last 100 years.

Keeping this unprecedented disaster in mind, we felt it is important to explore the possible mechanisms behind these events and to evaluate the fidelity of three state-of-the-art high-resolution deterministic and ensemble operational prediction systems with horizontal resolutions from 9 to 16 km. Namely the Integrated Forecast System (IFS) Ensemble Prediction System (EPS) from the European Centre for Medium-Range Weather Forecasts (ECMWF), the National Centers for Environmental Prediction (NCEP)-based Global Ensemble Forecast System (GEFS) being adopted and implemented by the Indian Institute of Tropical Meteorology (IITM), Pune, India, and operationally run by the India Meteorological Department (IMD), and last the Unified Model–based EPS from the National Centre for Medium Range Weather Forecast (NCMRWF). In particular, we want to explore the prediction horizon (lead time) for such events and evaluate the models ability to reproduce the dominant physical processes and large-scale atmospheric circulation patterns of these events.

Another catastrophic flooding during July 2010 over Pakistan was meticulously analyzed by Webster et al. (2011). The amount of rainfall during July 2010 over Pakistan was much lower than that over Kerala. Other extreme rain event in recent times occurred over the Uttarakhand, India, during 17 June 2013, which caused widespread damage and devastation to human lives and property. Studies by Dube et al. (2014), Joseph et al. (2015) and Pattanaik et al. (2015) showed that the event was well predicted by the extended-range prediction system based on CFS/GFS (CFS stands for Climate Forecast System, which is the coupled version of GFS). These analyses raise the hope that the models, particularly the ensemble systems have some fidelity in capturing the catastrophic rainfall over Kerala. Number of earlier studies e.g., Zhao et al. (2020); Vokoun and Hanel (2018) and the references there in, demonstrated the usefulness of ensemble systems in providing more skillful predictions at longer lead times and therefore help to reduce economic loss (Richardson 2000).

The paper is arranged with the description of the models, data, and methodology in sections 2–3. The synoptic conditions and observations are presented in section 4. Section 5 aims to explain the forcing and physical mechanism of the rain events based on ERA (ECMWF Reanalyses) analyses. The skill of the high-resolution deterministic and ensemble forecasts is discussed in sections 6 and 7, and a summary is given in section 8.

2. Observing convection

The India Meteorological Department at Kochi has a dual-polarization Doppler weather radar that operates at 2.832-GHz frequency, and it has a scan range ~240 km with scan resolution of 150 m and 10 scanning elevations from 0° to 20°. The radar has a pulse width of 1.0 ms. Images of radar reflectivities have been mainly used to understand the vertical extension of the convection.

Since 2018, IMD displays ground-based lightning data as a merged product with *INSAT-3D* satellite-based cloud information on an operational basis. The lightning flashes/strikes (cloud-to-ground) are recorded by the ground-based network. Lightning data are available every 2 min from the Indian Institute of Tropical Meteorology (IITM) lightning network and every 15 min from the Indian Air Force (IAF). For visualization, these flashes/strikes are categorized into different time slots (within the last 10–30 min) and superimposed on *INSAT-3D* cloud top temperatures.

The *INSAT-3D* (82°E) imager's thermal infrared channel at 10.8 μm (IR1) equivalent blackbody temperatures (BT) data are available every 30 min with subsatellite pixel resolution of 4 km × 4 km. The data have been retrieved for August 2018 and 2019 from the ISRO's Meteorological and Oceanographic Satellite Data Archival Centre (http://mosdac.gov.in) with the goal to delineate deep convective areas.

Scaife et al. (2017) argued the source of predictability of tropical rainfall could be derived from poleward-propagating Rossby waves. Many recent studies also suggest that Rossby waves favor the occurrence of extreme weather (Kornhuber et al. 2019; Screen and Simmonds 2014; Coumou and Rahmstorf 2012). While most of these studies refer to middle-latitude weather, we analyze tropical Rossby waves in relation to the extreme rain of August 2018 and 2019 over Kerala. The Rossby wave analysis is carried out following the methodology by Wheeler and Kiladis (1999). The Rossby part of the wave spectrum was extracted by filtering daily equatorial rainfall between 15°S and 15°N during JJAS. The filter window includes periods of 10–45 days, westward wavenumbers 1–10, and phase speeds corresponding to equivalent depths between 8 and 90 m.

3. Forecast models

a. GEFS modeling system

To develop a probabilistic block level (meteorological blocks are of the size of roughly 12 km × 12 km and several such blocks make a district and several districts make a state) forecast system over India, a very high-resolution ensemble

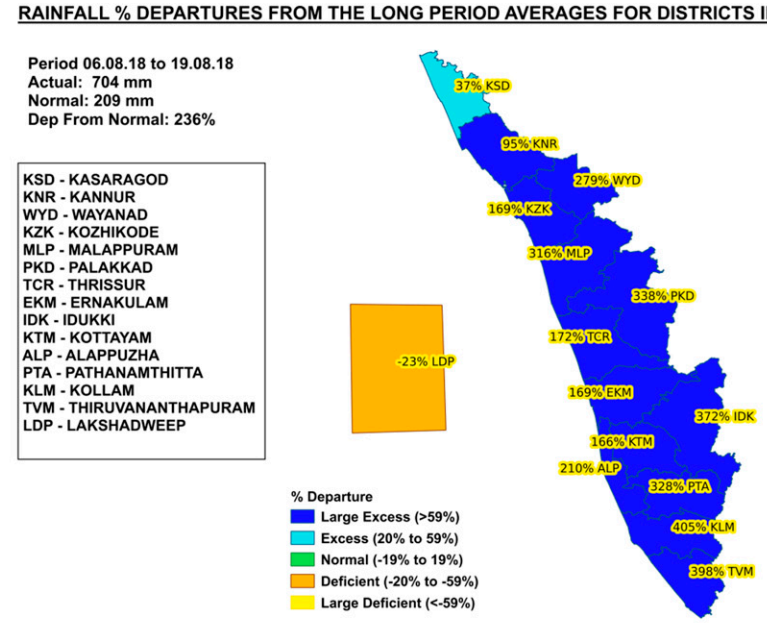

a)

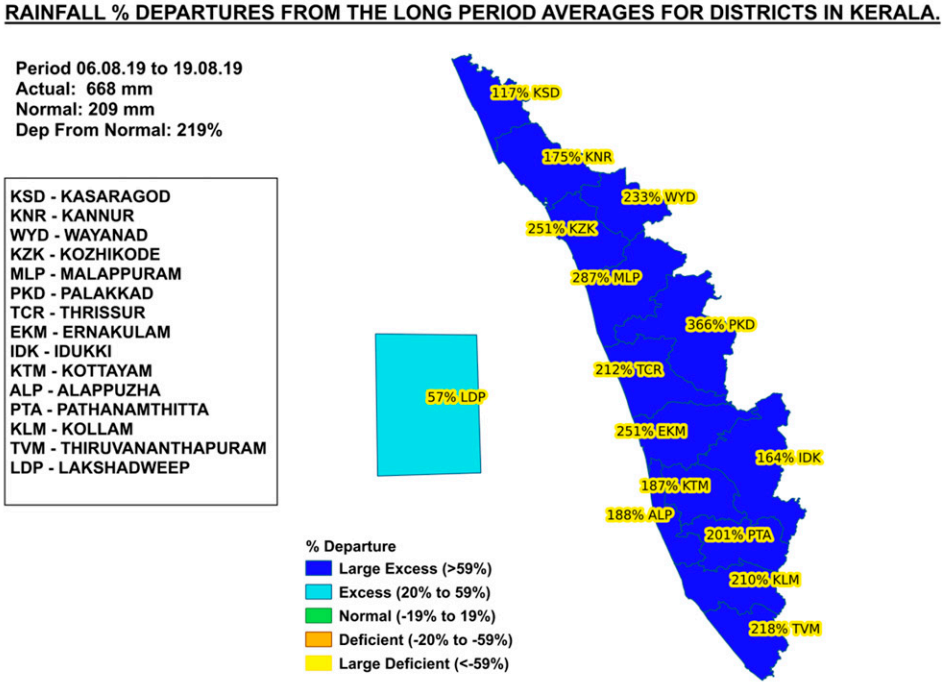

b)

FIG. 1. Rainfall departure over different districts of Kerala, India, during (a) 6–19 Aug 2018 and (b) 6–19 Aug 2019.

TABLE 1. Model specifications.

	GEFS	IFS	NEPS
Modeling center	IMD	ECMWF	NCMRWF
Ensemble members	21	51	21
Resolution	T1534 (3072 × 1536) ~12.5 km	~9 km	~12 km
Deep convection	Aerosol aware; deep convection (SAS) (Han and Pan 2011; Han et al. 2017)	Scale and Tiedtke scheme with Bechtold-based CAPE closure (Bechtold et al. 2014)	Mass-flux based (Gregory and Rowntree 1990)
Shallow convection	Scale- and aerosol-aware shallow scheme based on mass-flux (Han and Pan 2011; Han et al. 2017)	Tiedtke scheme with Bechtold-based CAPE closure (Bechtold et al. 2014)	Mass-flux based (Gregory and Rowntree 1990)
Microphysics	Zhao–Carr microphysics (Zhao and Carr 1997)	Forbes et al. (2011)	Wilson and Ballard (1999)
PBL	EDMF (Han et al. 2016)	EDMF (Han et al. 2016)	Lock et al. (2000)
Radiation	RRTM (Mlawer et al. 1997)	RRTM (Mlawer et al. 1997)	Radiation scheme of Edwards and Slingo (Edwards et al. 2018)
Surface model	Noah land surface model (Ek et al. 2003)	TESSEL scheme (Balsamo et al. 2009)	JULES (Best et al. 2011)

forecasting system with spectral resolution of T1534 (~12.5 km) and 64 hybrid vertical levels (top layer around 0.27 hPa) has been implemented for daily operational forecast since 1 June 2018. It is based on the global atmospheric model GFS as a global spectral (semi-Lagrangian grid) model (GSM) version 14.0.2 adopted from NCEP along with its 4D ensemble–variational (4D-Ens-Var) analysis system (Buehner et al. 2013; Kleist 2012; Kleist and Ide 2015). Thus, the prediction system is similar to that of the NCEP-GEFS (Zhou et al. 2016, 2017) system with the exception of the resolution of perturbed members, which are run at the same resolution of T1534 as the control member. Further modifications have been made to the analysis system to assimilate Indian satellite datasets, e.g., *Megha-Tropiques* Sounder for Probing Vertical Profiles of Humidity (MT-SAPHIR), *INSAT-3D* sounder radiances and atmospheric motion vectors (AMV) winds, *ScatSat-1* surface winds etc. With these enhanced analyses, the GEFS V14.0.2 aims to provide daily 10-day probabilistic forecasts using a 21-member (20 perturbed + 1 control) ensemble system initialized at 0000 UTC. Table 1 describes the GFS T1534 model physics.

b. *ECMWF IFS prediction system*

The ECMWF high-resolution forecast is run twice daily for 10 days on a cubic octahedral grid of truncation TCo1279 (~9 km) with 137 vertical levels extending up to 1 Pa. The time step is 450 s. The ensemble system comprises 50 members and is run twice daily on 91 vertical levels (also extending up to 1 Pa) at resolution of TCo639 (~18 km) and a time step of 720 s until day 15. Twice weekly the ensemble forecasts are extended from day 15 to day 46 at a reduced resolution of TCo319 (32 km). The ensemble is initialized from 25 independent 4D variational analyses that are generated using perturbed observations and

TABLE 2. Rainfall statistics [climatological mean, actual mean, and climatological and actual standard deviation (SD)] based on various IMD in situ station data over Kerala, India, during 6–19 Aug of 2018 and 2019.

	1961–2010		6 Aug 2018–19 Aug 2018		6 Aug 2019–19 Aug 2019	
	Climatological mean (mm)	Climatological SD (mm)	Actual mean (mm)	Actual SD (mm)	Actual mean (mm)	Actual SD (mm)
Kerala	14.95	1.12	50.29	41.67	47.74	44.73
Alappuzha	11.21	1.38	34.76	31.25	32.33	28.48
Ernakulam	14.25	1.61	38.31	46.78	50.08	46.25
Idukki	19.94	1.99	94.09	74.47	52.65	54.22
Kannur	19.39	1.74	37.97	32.16	53.49	49.30
Kasaragod	23.52	2.87	32.24	22.22	51.26	46.18
Kollam	8.22	1.11	41.58	37.59	25.56	24.07
Kottayam	13.19	2.08	35.16	29.82	37.91	31.36
Kazhikode	18.73	2.74	50.48	54.31	65.79	72.00
Malappuram	13.97	1.33	58.21	52.12	54.12	59.49
Palakkad	12.00	1.11	52.61	50.82	55.99	76.67
Pathanamthitta	11.10	1.20	47.59	42.21	33.42	32.62
Tiruvananthapuram	4.62	0.86	23.02	26.50	14.71	18.46
Thrissur	16.88	2.13	45.92	64.83	52.78	49.50
Wayanad	19.97	3.47	64.78	49.89	66.64	78.95

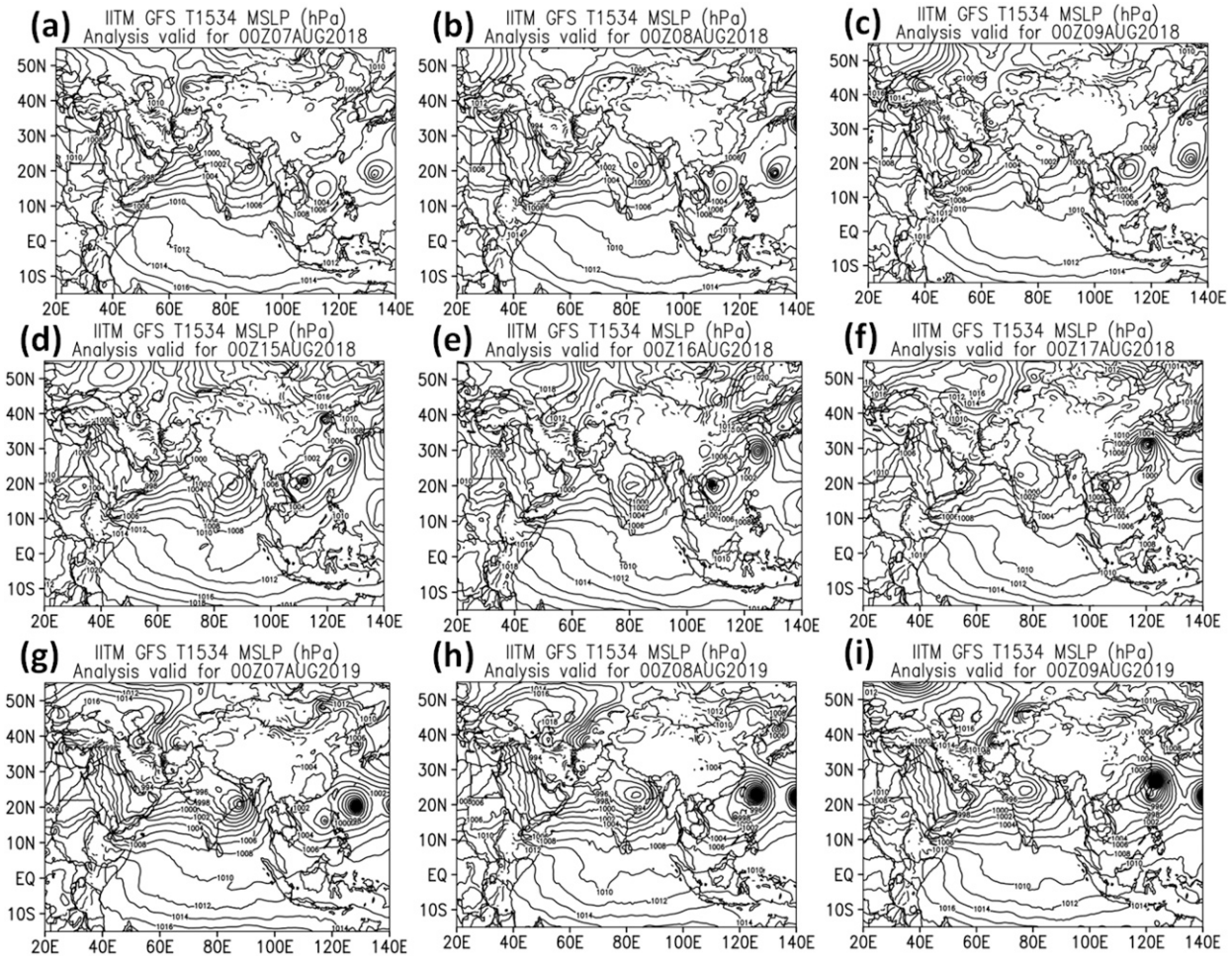

FIG. 2. The GFS model analyses for (a)–(c) 7–9 Aug 2018, (d)–(f) 15–17 Aug 2018, and (g)–(i) 7–9 Aug 2019, depicting the monsoon depression and its position.

perturbed forecasts with perturbations of the total physics tendencies. The 50 different initial states are generated by centering the 25 perturbed analyses around the high-resolution analysis and applying the resulting pairs of positive and negative anomalies and adding also moist singular vector perturbations.

c. *NCMRWF Unified Model*

The NCMRWF Unified model (NCUM) is a global model and has a horizontal grid resolution of ~12 km with 70 levels in the vertical reaching 80-km height. It uses the ''ENDGame'' dynamical core (Kavčič and Thuburn 2018; Walters et al. 2017), which provides improved accuracy of the solution of primitive model equations and reduced damping. This helps in producing finer details in the simulations of synoptic features such as cyclones, fronts, troughs, and jet stream winds. The time step is 5 min and coupled to the JULES (Joint U.K. Land Environment Simulator) land surface model, which produces improved near surface features. The ENDGame core also increases variability in the tropics, which leads to an improved representation of tropical cyclones and other tropical phenomena (Walters et al. 2017).

The model orography is derived from the Global Land One-km Base Elevation Project (GLOBE) data. The deep convection is mass flux scheme based on Gregory and Rowntree (1990) but having several modifications including the CAPE closure with a fixed CAPE time scale. Diagnosis of shallow or deep convection is made by the boundary layer turbulence parameterization, which is a first-order turbulence closure based on Lock et al. (2000). It has mixed-phase microphysics (based on Wilson and Ballard 1999), diagnostic cloud scheme (Smith 1990), radiation (based on Edwards and Slingo 1996), land surface scheme (Best et al. 2011), and orographic gravity wave drag parameterization basically designed by Lott and Miller (1997). The prognostic dust aerosol is also included with a scheme based on Bellouin et al. (2011). A technical report by Kumar et al. (2018) describes in detail the operational implementation of NCUM at NCMRWF.

The operational NCMRWF Ensemble Prediction System (NEPS) has 22 ensemble members. The horizontal resolution of NEPS is ~12 km. The initial condition perturbations of this ensemble prediction system are generated by the ensemble transform Kalman filter (ETKF) method (Bowler et al. 2009),

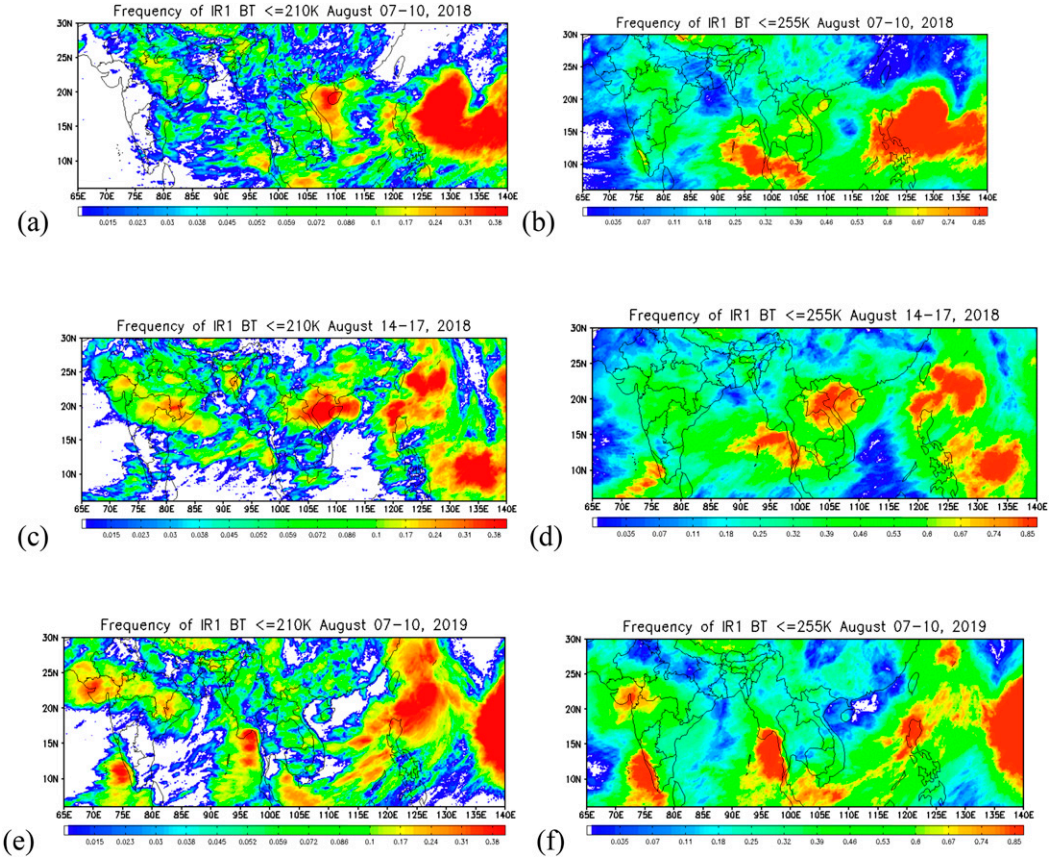

FIG. 3. Frequency of brightness temperature (left) ≤210 K and (right) ≤255 K for (a),(b) 7–10 Aug 2018; (c),(d) 14–17 Aug 2018; and (e),(f) 7–10 Aug 2019.

and model uncertainties are taken care of by the stochastic kinetic energy backscatter and random parameters schemes (Tennant et al. 2011). The forecast perturbations obtained from a 6-h short forecast run of 22 ensemble members are updated by ETKF four times a day (0000, 0600, 1200, and 1800 UTC). Perturbations of surface parameters such as sea surface temperature, soil moisture content and soil temperature (Tennant and Beare 2014) are included in the 12-km NEPS in order to address the problem of lack of ensemble spread near the surface. The NEPS aims to provide 10-day probabilistic forecasts using 23 members (22 perturbed + 1 control) ensemble system. Out of 22 perturbed ensemble members, one set of 11 members is run from 0000 UTC and the other set of 11 members is run from 1200 UTC to provide ensemble forecast for 10 days. The operational deterministic forecast running at 12-km resolution from 0000 UTC is used as the control forecast. A technical report by Mamgain et al. (2018) describes in detail the operational implementation of this high-resolution NEPS.

4. The Kerala heavy rain events

a. Reported extreme rain during 2018 and 2019

The districts of Kerala state and the rainfall departures from long-term daily climatological values as observed by IMD during 6–19 August 2018 and 2019 are shown in Figs. 1a and 1b. During the 2018 event, most of the districts of Kerala received very high amounts of rain with departures from climatology of ~100%, with some showing departures up to 300%–400%. The only district with below normal rainfall is KSD (Kasaragod) the extreme north of the state (Fig. 1a) that received only 50% of its climatological value. During the 2019 event, departure of the rainfall during 6–19 August over the state was more than 200%. However, no districts show 400% departures as in 2018 and only the Palakkad districts show a departure of more than 300% (366%). Table 2 further indicates the quantitative rainfall statistics over Kerala during 6–19 August of 2018 and 2019 based on in situ station data. The majority of the stations show that the standard deviation (SD) of the actual rainfall is more than 30–50 times of the climatological SD during 6–19 August of 2018 and 2019.

During 8–9 August 2018, a monsoon depression was moving across the Indian subcontinent from the head of the Bay of Bengal in a northwestward direction. Another monsoon depression formed over the head of the Bay of Bengal and moved northwestward during 14–18 August 2018. The GFS analyses for 7–9 August and 15–17 August 2018 depict the monsoon depression and its position (Fig. 2). During 7–10 August 2019, a monsoon depression formed over the head of the Bay of Bengal

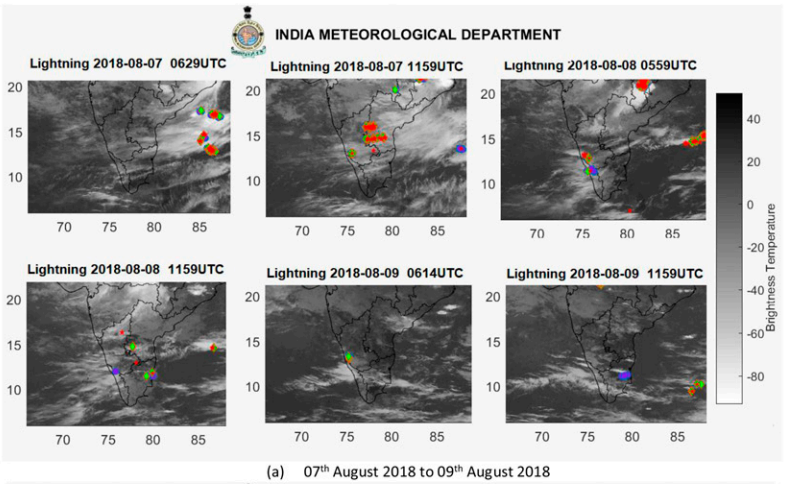

(a) 07th August 2018 to 09th August 2018

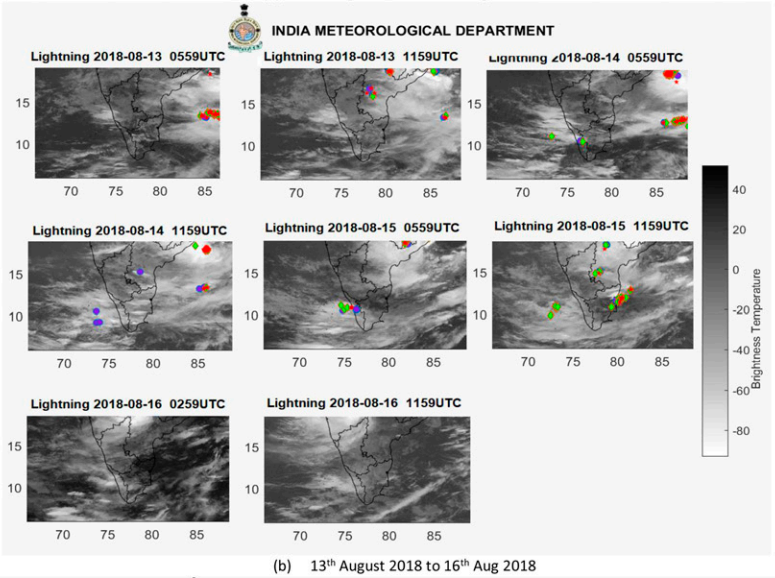

(b) 13th August 2018 to 16th Aug 2018

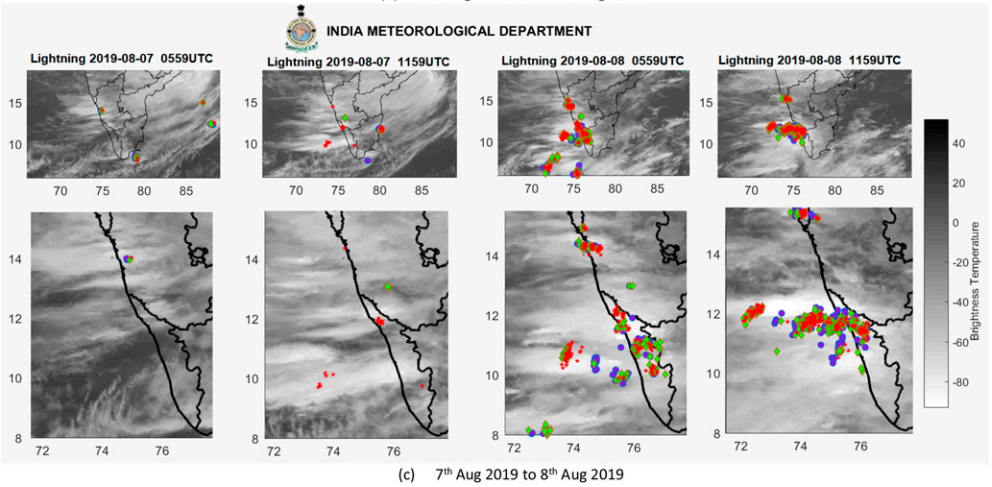

(c) 7th Aug 2019 to 8th Aug 2019

FIG. 4. The cloud brightness temperature from the *INSAT-3D* satellite and associated lightning flashes for (a) 7–9 Aug 2018, (b) 13–16 Aug 2018, and (c) 7–9 Aug 2019.

and was crossing the Indian landmass from the southeast in a northwestward direction. The GFS analyses capture the position of the monsoon depression on 7–9 August 2019 (Figs. 2g–i). It is evident that all monsoon depressions moved in the northwestward direction. Interestingly, during the passage of the monsoon depressions, large-scale organization of tropical disturbances was observed, with the formation of two tropical cyclones over the western Pacific (Figs. 2g–i).

b. Assessment using INSAT-3D *products*

To characterize the type of convection associated with these rainfall episodes, we use brightness temperatures of the *INSAT-3D* satellite for the period 7–10 August and 14–17 August 2018 (Figs. 3a–d). The IR1 pixels with BT lower than 210 K are generally associated with deep convective systems, while BTs in the range of 240–255 K are considered as cumulus congestus and convective debris, i.e., anvil/cirrus (Roca et al. 2002). Figure 3 shows the frequency of pixels within a grid box of 0.1° × 0.1° that were observed during the heavy rain spells with BTs less than 210 and 255 K, respectively. Temperatures ≤ 210 K occur with very low frequency over the Kerala region during the mentioned periods, although temperatures lower than 255 K are noticeable over the state. It can therefore be inferred that the rain was mostly from cumulus congestus or shallow convective clouds. For the episode 7–10 August 2019 the frequency of BTs ≤ 210 and ≤255 K are illustrated in Figs. 3e and 3f. The convection during this period over the Kerala region and nearby ocean is also dominated by congestus or shallow convective clouds. However, with a frequency exceeding 30% there are significantly more deep convective clouds than during the 2018 event.

Satellite (*INSAT-3D*) cloud top temperature and associated lightning data over Kerala are displayed in Fig. 4. It is evident from the satellite imageries of 7–9 August 2018 (Fig. 4a) and 13–16 August 2018 (Fig. 4b) that the Kerala region is mostly dominated by shallow clouds, with occasional presence of deep convection during the heavy rainfall episodes. Only few lightning flashes are recorded during the extremely heavy rainfall episodes, which reconfirms that the rainfall events are associated with shallow and congestus convection. The brightness temperature superimposed with the lightning flashes during 7–8 August 2019 are displayed in Fig. 4c. Significant lightning activity is observed at 1130 UTC 8 August 2019, but only few lightning flashes for 7 August 2018.

An additional analysis on the total number of lightning strikes per area (not shown) revealed that the whole state of Kerala experienced significantly less lightning than the region affected by the monsoon depression, with the lightning flash count around the monsoon depression being two orders of magnitude higher than over Kerala. Interestingly, the lightning flashes over Kerala were particularly reduced on 15 August 2018 when the state registered the strongest rainfall in August 2018.

c. Assessment using radar products

Figure 5 shows the spatial and vertical cross section of maximum radar reflectivity (MaxZ). It shows the maximum amount of returned power to the radar from a certain height that can be deduced from the top and right plots. The top plot in each panel of Fig. 5 measures the maximum reflectivity at

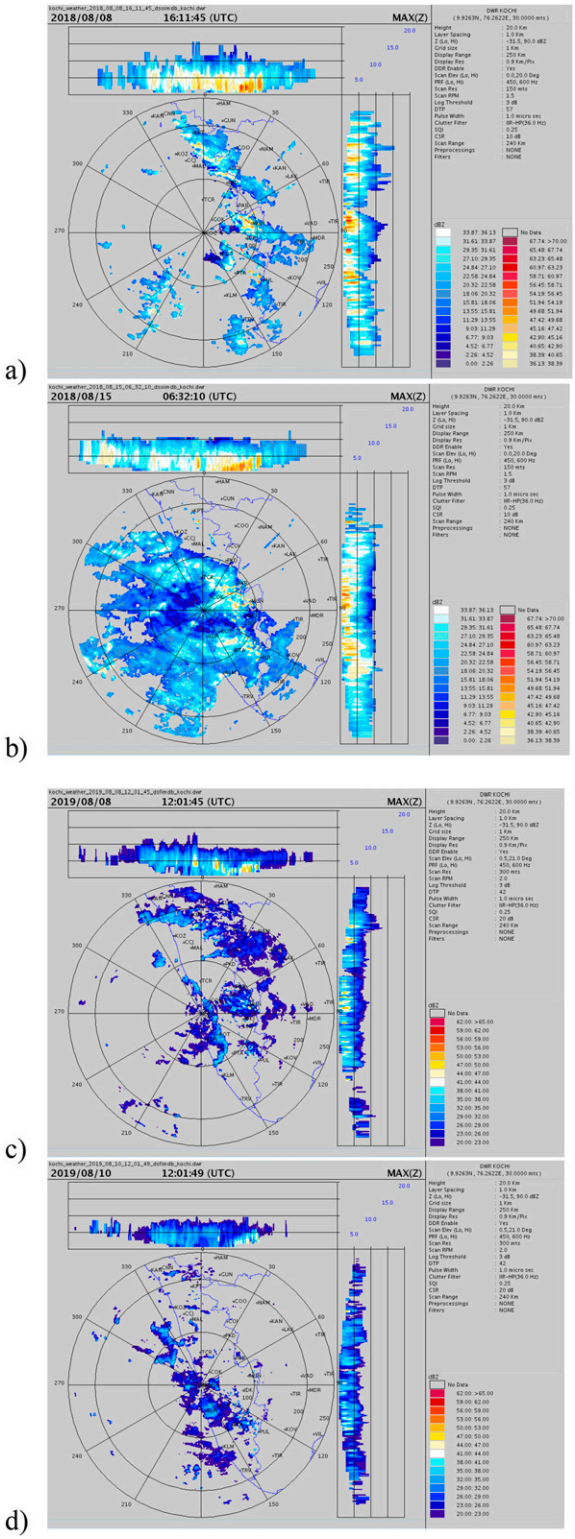

FIG. 5. Radar images of MaxZ (dBZ) over Kochi for (a) 8 and (b) 15 Aug 2018 and (c) 8 and (d) 10 Aug 2019.

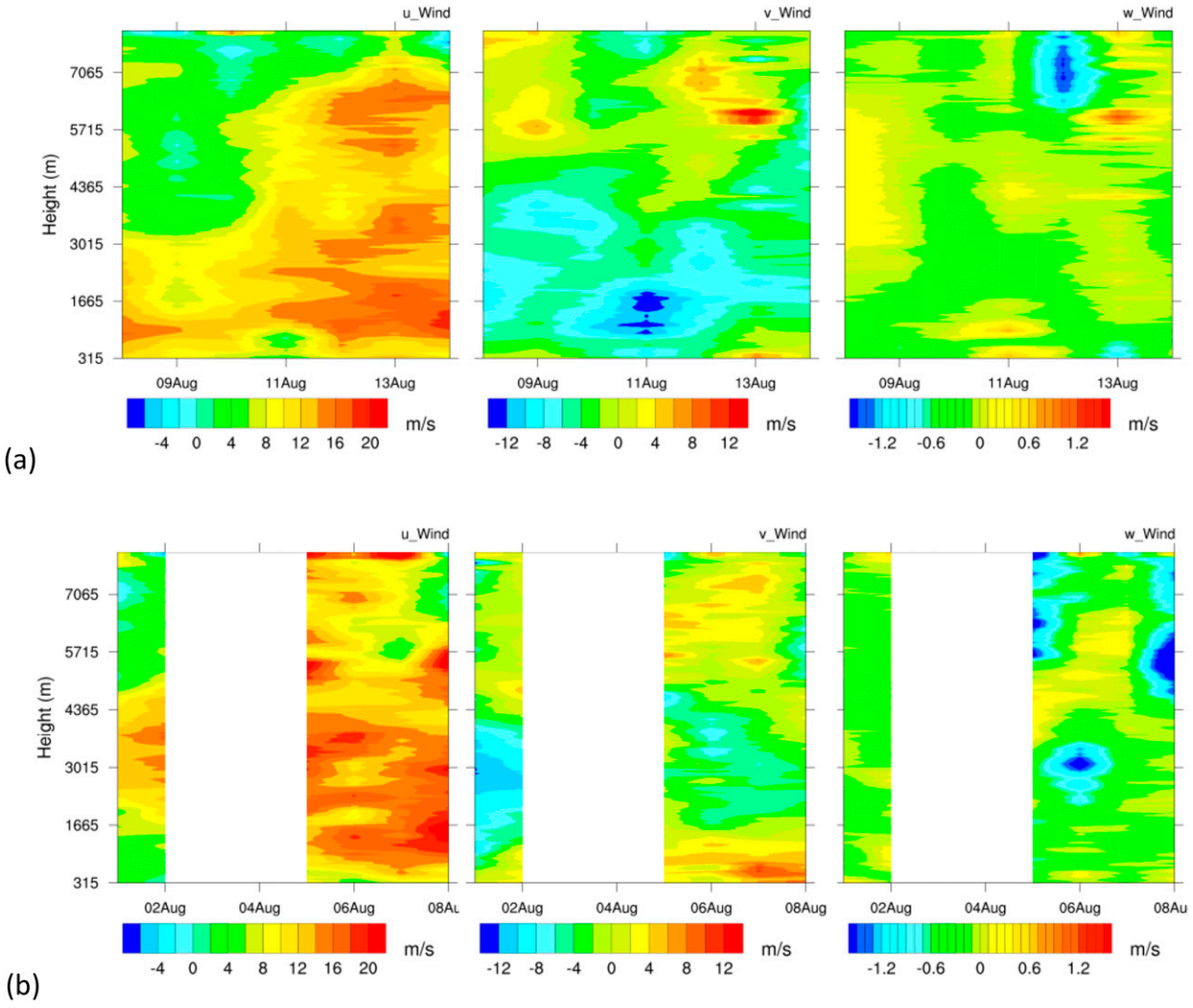

FIG. 6. (left) Zonal, (center) meridional, and (right) vertical component of wind during (a) 8–14 Aug 2018 and (b) 1–8 Aug 2019 from the wind profiler in Kochi.

each level starting from ground to top when we look in the north–south direction. Likewise the right side plot in each panel shows the maximum reflectivity at each level when we look from west to east. Overall the MaxZ plot shows the three-dimensional view of the maximum reflectivity observed in the region of our interest.

The radar observed MaxZ values also confirm that clouds are confined within the lower troposphere up to around 4 km (Figs. 5a,b) over Kochi on 8 and 15 August 2018. Figures 5c,d shows the MaxZ for the dates 8–10 August 2019, where MaxZ is confined within 5 km. Overall, the reflectivity values are around 30–35 dBZ with MaxZ being associated with heights below 10 km in most cases.

In addition, the observed vertical wind component (right panel of Figs. 6a,b) is shown from the wind profiler located at Kochi for the period of 8–14 August 2018 and 1–8 August 2019. The wind profiler shows predominance of weak vertical velocities during 8–14 August 2018 and during 6–8 August 2019. The wind profilers indicate, however, the presence of a strong lower-level zonal flow (Figs. 6a,b) during both August 2018 and August 2019.

5. Moisture budget and large-scale forcing

a. Moisture convergence

The observation-based analyses primarily indicate that the extremely heavy rain of August 2018 and 2019 has not been contributed by the deep convection but by orographically strengthened shallow and mesoscale convection. This perplexing observational evidence, and particularly the wind profiler observations, prompts us to further investigate the hypothesis whether the strong lower level moisture advection and associated large-scale features are responsible for the unprecedented heavy rain. To test this hypothesis, a water vapor budget (WVP) equation following Yanai et al. (1973) has been applied. The vertically integrated moisture convergence and tendency of total column water is averaged over 73°–78°E, 8°–13°N and plotted in Fig. 7 for GFS, IFS,

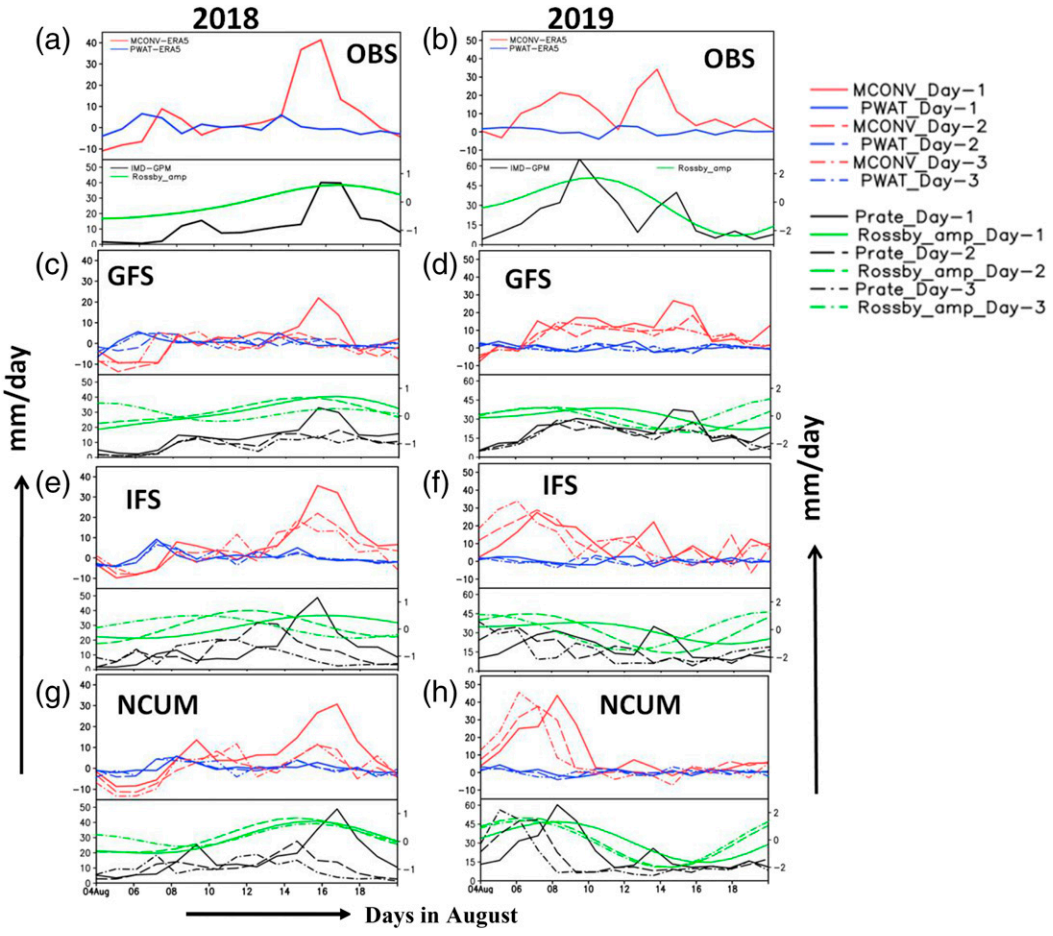

FIG. 7. The top part of each panel is the vertically integrated moisture convergence (mm day^{-1}) and precipitable water vapor (mm day^{-1}) for (a) August 2018 and (b) August 2019 over Kerala and the adjacent region (73°–78°E, 8°–13°N). The bottom part of (a) and (b) shows the observed IMD-GPM merged gridded rainfall data (black; mm day^{-1}) and Rossby amplitude (green; mm day^{-1}) for August in (left) 2018 and (right) 2019. (c) Moisture convergence (red) and precipitable water vapor (blue) with day 1, 2, and 3 lead by GFS for August 2018. (d) As in (c), but for August 2019; (e) as in (c), but with IFS; (f) as in (d), but with IFS; (g) as in (c), but with NCUM; and (h) as in (d), but with NCUM.

and NCUM forecast with different lead times and is compared to ERA5 as the observational counterpart. The left panel of Fig. 7 is for August 2018 and the right panel for August 2019. It is evident from the ERA5 analyses (Fig. 7a, top panel) that the vertically integrated moisture convergence was high on 8 August and significantly above average on 15 and 16 August 2018. Total column precipitable water tendency remains low throughout during 4–19 August, indicating a possible major contribution of moisture convergence to the extreme precipitation. Strong moisture convergence is well correlated with excessive precipitation, as indicated by the black lines in the lower sub panels. Interestingly, the Rossby wave amplitude (green lines in lower subpanels) also reaches its peak during 15–16 August 2018 coinciding with the moisture convergence maximum (upper panel of Fig. 7a).

b. *Barotropic Rossby wave and the heavy rainfall of August 2018–19*

Apart from the moisture and Rossby amplitude analyses, we intend to investigate the extreme events as a manifestation of tropical wave propagation particularly the westward-propagating Rossby wave. We hypothesize whether the events are associated with the westward-propagating Rossby wave during August 2018 and 2019. The Rossby wave analysis follows the methodology proposed by Wheeler and Kiladis (1999). The Rossby part of the wave spectrum is extracted by filtering daily equatorial rainfall between 15°S and 15°N during JJAS. The filter window includes period 10–45 days, westward wavenumber 1–10, and equivalent depth between 8 and 90 m.

Analyzing the rainfall time series in Fig. 7 in terms of Rossby wave amplitude, we demonstrate that all three models capture the moisture convergence and high Rossby amplitude for 15–16 August 2018 at day-1 lead. However, for lead times day 2 onward the moisture convergence and precipitation in the forecasts reduces and a phase shift appears in the Rossby amplitude, particularly in the IFS model. For the latter, the Rossby wave is more in phase with the convergence compared to the other models. For the 8–10 August 2019 event, NCUM and IFS produce a strong moisture convergence signal that is in

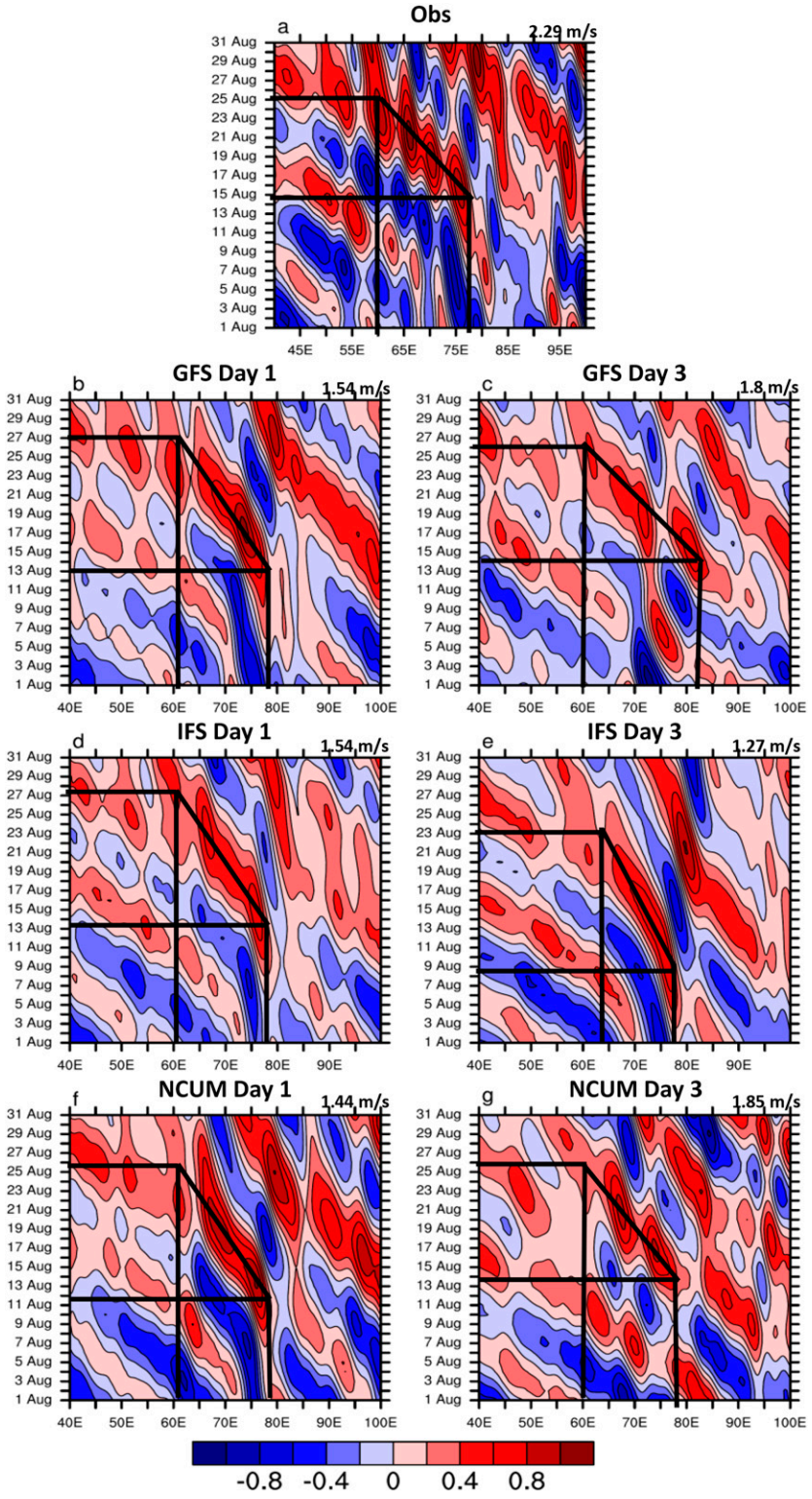

FIG. 8. Rossby wave–filtered precipitation anomaly (mm day^{-1}) of August 2018 from (a) observations; (b),(c) GFS; (d),(e) IFS; and (f),(g) NCUM. Day-1 forecasts are shown in (b), (d), and (f), and day-3 forecasts are shown in (c), (e), and (g).

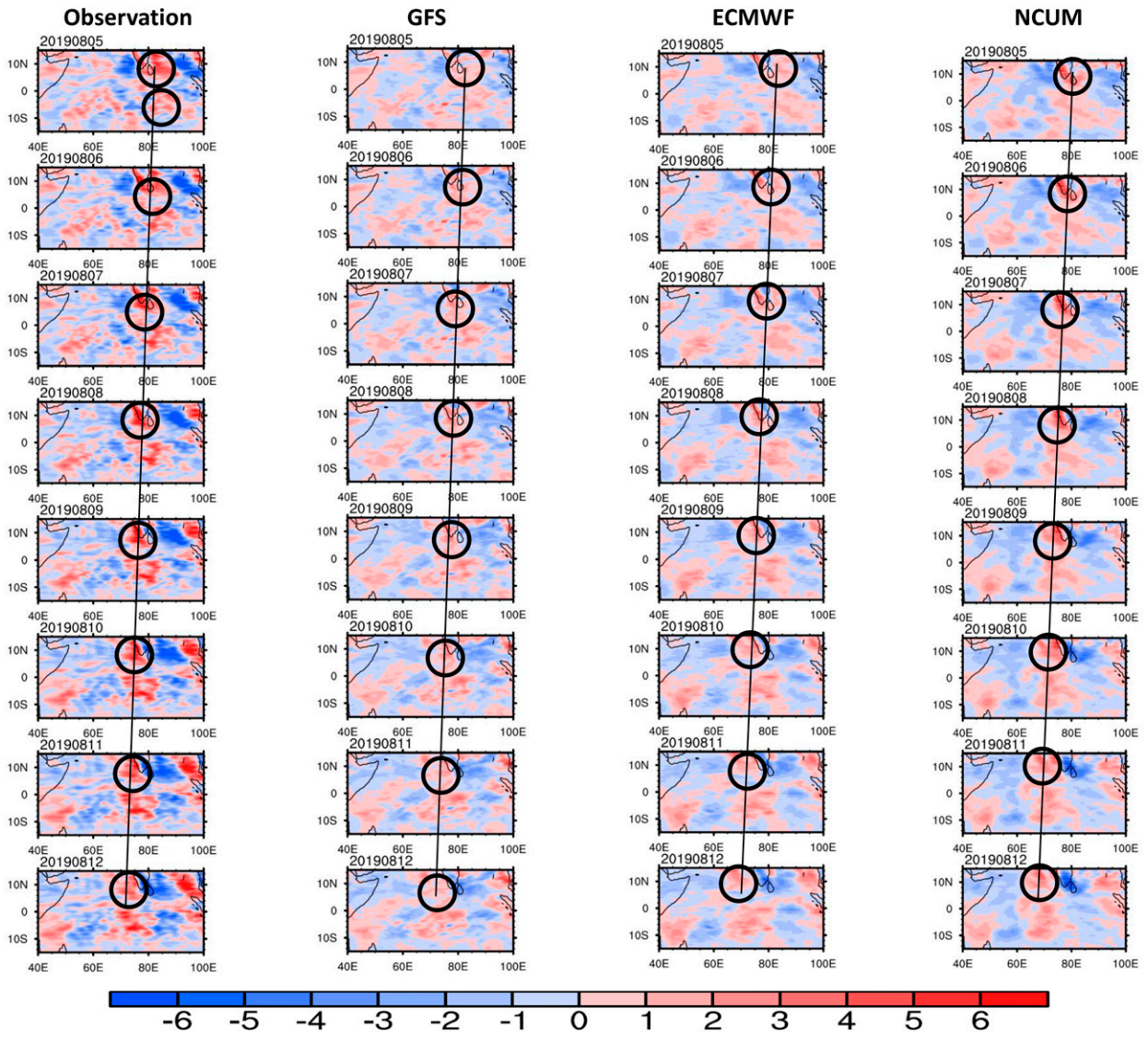

FIG. 9. Spatial structure of westward-propagating Rossby wave–filtered precipitation anomaly (mm day^{-1}) from (from left to right) observation and from day-1 forecasts of GFS, IFS, and NCUM, respectively.

line with the ERA5, while GFS produces a much weaker signal with an actual maximum on 15 August 2019. Anomalously high moisture convergence and rainfall predictions are maintained by the IFS and NCUM forecasts at lead day 2–3 together with a realistic Rossby wave amplitude, albeit a small phase shift. The Rossby wave amplitude and precipitation are weaker in the GFS that produces the main precipitation at 14 August 2019 that corresponds in the ERA5 to the day in August 2019 with the largest moisture convergence, but only moderate Rossby amplitude.

Figure 8a displays Hovmöller diagrams of the Rossby wave–filtered precipitation anomaly for August 2018. Two major westward-propagating signals are evident. The signal with the largest positive anomaly is initiated on 7 August around 80°E and reaches Kerala around 76°–77°E during 14–17 August, the phase speed is around 2 m s^{-1}. The GFS day-1 forecast (Fig. 8b) reproduces the westward-propagating signal with highest amplitude on 16–18 August over Kerala, but by day 3 the signal appears to have weakened and westward propagation is not well organized. The phase speed of the westward-propagating Rossby wave in GFS is ~1.5 and 1.8 m s^{-1} in day-1 and day-2 forecasts, respectively, and, therefore, lower than the observed value of 2.29 m s^{-1}. The IFS consistently captures the Rossby wave signal at day-1–3 lead, albeit with a stronger amplitude at day 3, while Rossby wave phase speeds are underestimated (1.5 m s^{-1} at day 1 and 1.2 m s^{-1} at day 2). NCUM captures the Rossby waves at day 1, but these become disorganized by day 3, where phase speeds attain 1.4 and 1.8 m s^{-1}, respectively.

A much clearer picture is obtained for August 2019 (figure not shown). The observations show two major westward-propagating

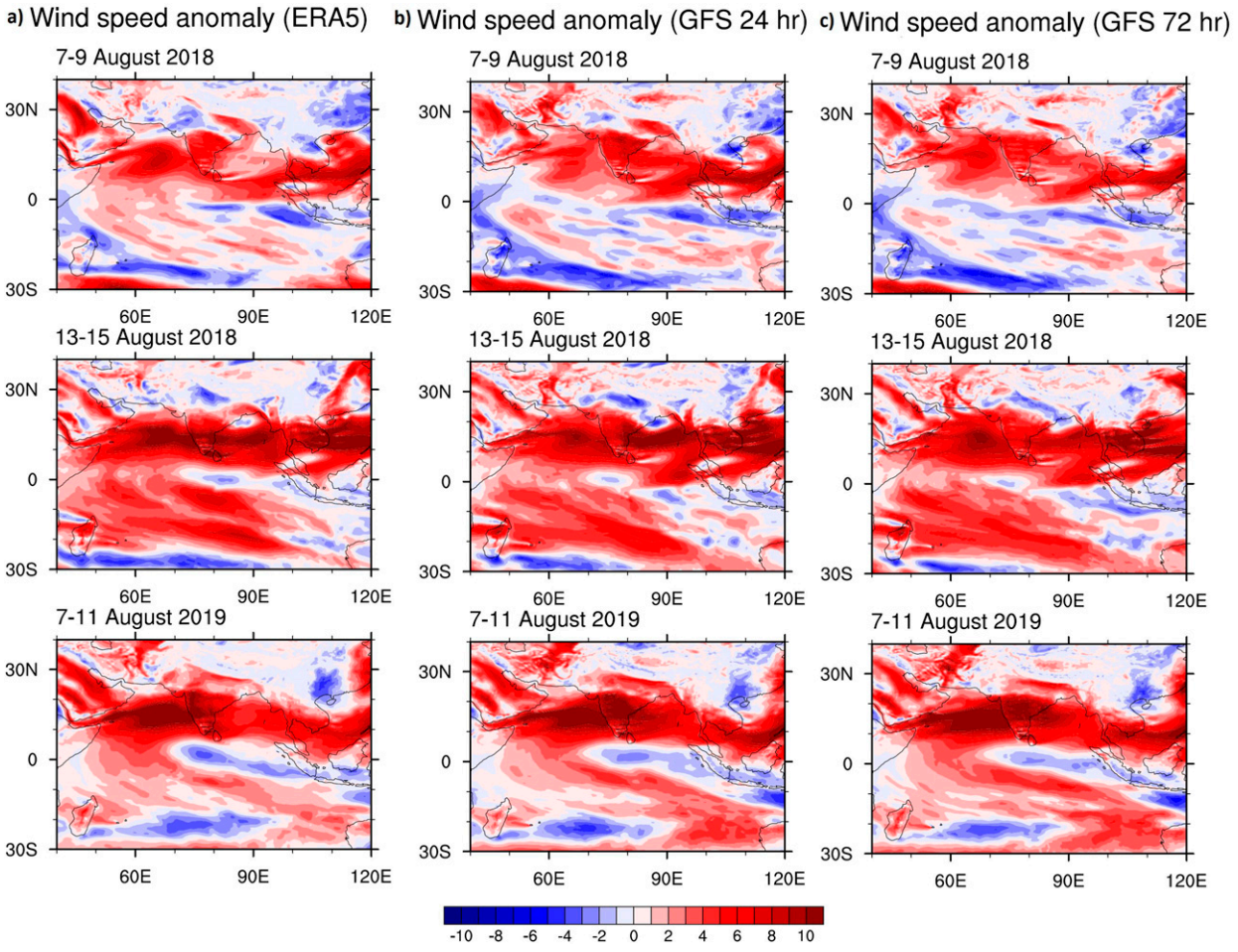

FIG. 10. The 850-hPa wind speed anomaly from (a) the ERA5 and (b),(c) from day-1 and day-3 forecasts with the GFS.

signals, the major signal emerges at 90°E around 1 August and approaching Kerala by about 8–10 August 2019. Here, the IFS and NCUM realistically reproduce the Rossby wave signal at day-3 lead, while the amplitude is significantly reduced in GFS at day 3. The phase speed of the Rossby wave during August 2019 is found to be around $\sim 2\ \mathrm{m\ s^{-1}}$ and is reasonably captured by the models. More insight is gained by the spatial distribution of the Rossby wave during 5–12 August 2019 which is shown in Fig. 9. All three models have reasonably capture the westward propagation of the Rossby wave during 5–12 August 2019 with some underestimation in amplitude by GFS and IFS as compared to the observations.

Finally, the large-scale wind anomalies are shown in Fig. 10 as computed from ERA5. It is evident that on the days of extreme events of August 2018 and 2019, there was a large-scale anomalously strong wind at 850 hPa (maxima of low level monsoon jet) triggered by anomalously strong sea level pressure gradient reasonably reproduce the anomalies in the ERA5.

In summary, this analysis suggests that the westward-propagating Rossby waves and associated moisture advection play an important role in triggering and sustaining the extreme rain events during August 2018 and 2019. Models have better captured the westward propagation for August 2019 than for August 2018 at day-3 lead.

6. Evaluation of operational deterministic forecasts

The rainfall averaged over the land portion of Kerala region from the India Meteorological Department-Global Precipitation Measurement (IMD-GPM) merged gridded observations and deterministic forecast from different models is shown in Fig. 11. IMD-GPM rain is derived from observed satellite (GPM) gauge merged gridded rainfall data at 25-km grid (Mitra et al. 2009). The GFS hardly captures the first heavy rainfall episode on 8 and 9 August (Fig. 11a), while the heavy rain episode on 15–16 August is captured at day-1 lead, only. Similarly, the IFS (Fig. 11b) misses the 8–9 August event, but reasonably captures the 15–16 with a lead of day 2. However, NCUM was able to predict the amplitude during 8–9 August at day-1 lead (Fig. 11c) and similarly performed to GFS and IFS for the 15–16 August, while overestimating the rainfall on 17 August. It can be said that for all models there is marked reduction in forecast precipitation by day 3, beyond that the forecasts. Finally, note that during the 10–13 August period, the rain intensity is still well above the daily

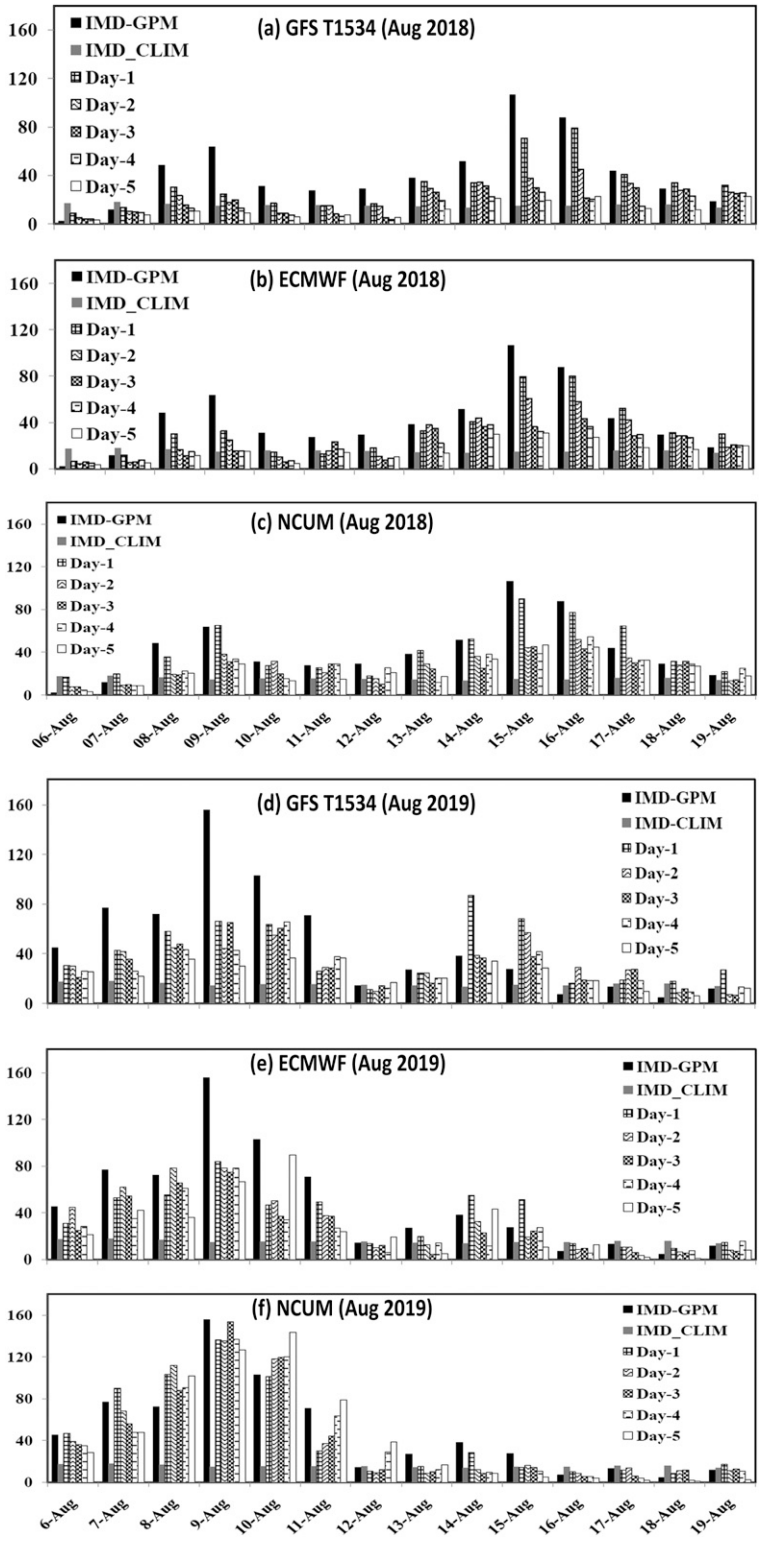

FIG. 11. Time series of rainfall (mm day^{-1}) averaged over state of Kerala for (a) GFS, (b) ECMWF, and (c) NCUM forecasts at various lead times (day 1–day 5) for 6–19 Aug 2018. (d)–(f) As in (a)–(c), but for 6–19 Aug 2019.

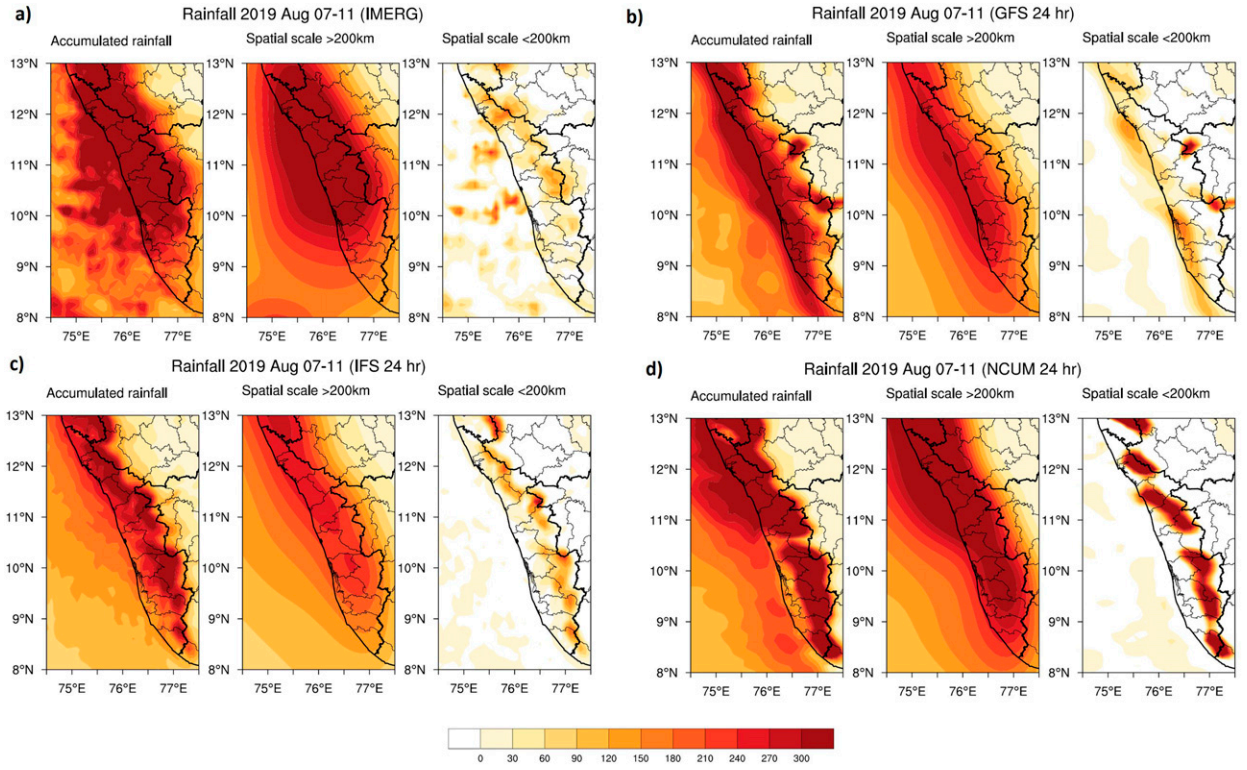

FIG. 12. Spatial-filtered rainfall distribution: (left) total rainfall, (center) rainfall from the large scale (>200 km), and (right) rainfall from the smaller scale (<200 km) for the period 7–11 Aug 2019 (a) IMERG; (b) as in (a), but for GFS 24-h lead; (c) as in (a), but for IFS 24-h lead; and (d) as in (a), but for NCUM 24-h lead forecast.

climatology, but the models generally also underestimate the precipitation during this period.

Considering August 2019 (Figs. 11d,e), GFS and IFS significantly underestimate the observed rainfall during 7–10 August, while NCUM reasonably captures the observed rainfall. Interestingly, in NCUM the rainfall tends to increase with lead time, contrary to the other models, where rainfall intensity generally decreases with lead time. Overall, the rainfall predictions of the different models are consistent with the evolution of the moisture convergence in Fig. 7.

To further highlight the fidelity of the three modeling systems in predicting the precipitation patterns contributing to the extreme events of August 2018 and 2019. In Fig. 12a the low-/high-pass-filtered precipitation from GPM (IMERG) and model forecasts for scales > 200 km (large-scale) and scales < 200 km (mesoscales) has been plotted for 7–11 August 2019. Shown are the spatial filtered rainfall distribution (Fig. 12a) IMERG total rainfall (left panel), rainfall from large scale (>200 km; center panel), and rainfall from the smaller scale (<200 km; right panel) for the period 7–11 August 2019; Fig. 12b is as in Fig. 12a, but for GFS 24-h lead; Fig. 12c is as in Fig. 12a, but for IFS 24-h lead; and Fig. 12d is as in Fig. 12a, but for NCUM 24-h lead forecast. To separate the contribution of rainfall coming from the large scale (i.e., >200 km), a Lanczos low-pass filter is applied in the latitudinal and longitudinal directions (Duchon 1979). Contribution of rainfall from smaller scales (i.e., spatial scales < 200 km) is the difference between the total field (raw data of rainfall) and low-pass-filtered data. The dominant contribution to the rainfall is shown to come from the large scales. A similar filter has been applied to the forecast models in Fig. 12 for the event of 7–11 August 2019. All models have been able to reasonably predict the large-scale rainfall as seen in the observation (>200-km scale). The models also have captured the mesoscale contribution for all three events (figure for August 2018 not shown) as compared to the observations. Note that in some cases IMERG data underestimate extreme rain events.

7. Evaluation of operational probabilistic rainfall predictions over Kerala

Ensemble prediction systems are expected to provide more skillful longer-range forecasts than the single high-resolution forecasts and also inform about the uncertainty of the forecasts. Earlier studies (Webster et al. 2011) showed the usefulness of ECMWF ensemble forecast during Pakistan flood event of 2010.

The IMD-GPM observed rainfall for 13–16 August 2018 and the ensemble mean accumulated rain from forecasts starting 12 August are illustrated in Fig. 13. The ensemble forecast systems are the GFS (GEFS), the ECMWF IFS ensemble prediction system and NCMRWF-generated Unified Model–based EPS (NEPS). Broadly speaking, the NEPS has captured the spatial rainfall distribution although with more orographically

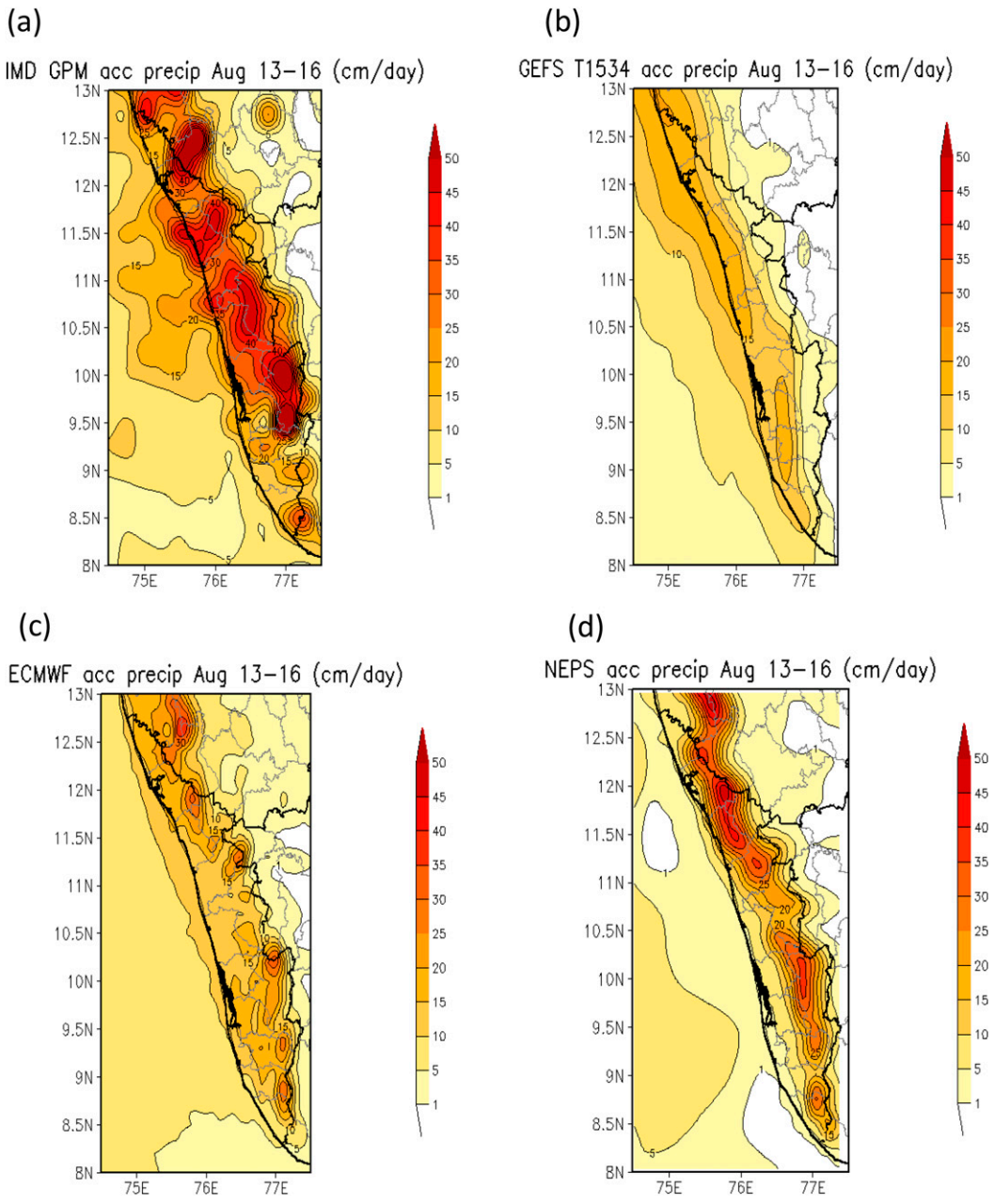

FIG. 13. Precipitation (cm day^{-1}) accumulated during 13–16 Aug 2018 from (a) IMD-GPM along with ensemble mean precipitation forecasts starting at 0000 UTC 12 Aug 2018, (b) GEFS, (c) ECMWF, and (d) NEPS.

enhanced rainfall near the Western Ghats, while GEFS appears to produce more rain over the oceanic region. The IFS captured the overall rainfall distribution but with some significant underestimation during both periods.

We also show the 7–11 August 2019 event in Fig. 14. The observations (Fig. 14a) show widespread and extreme rainfall across Kerala. The models performs quite similarly as for the 2018 event with more coastal rainfall in the GEFS, more realistic inland precipitation in the IFS, but underestimation over the orography, and overall strong orographic rainfall in NEPS in 2019 with an overestimation in the southern Ghats.

To explore the probabilistic predictions, we first consider the probability of rainfall exceeding the threshold of one SD above the observed climatology. The daily climatological value for Kerala is around 20 mm day^{-1} with one SD corresponding to 15 mm day^{-1}. Using probability of occurrence of 50% as a measure, it is shown in the first column of Fig. 15 that for 15 August 2018 all model forecasts are skillful up to 5 days. Increasing the rainfall threshold further to two SD the

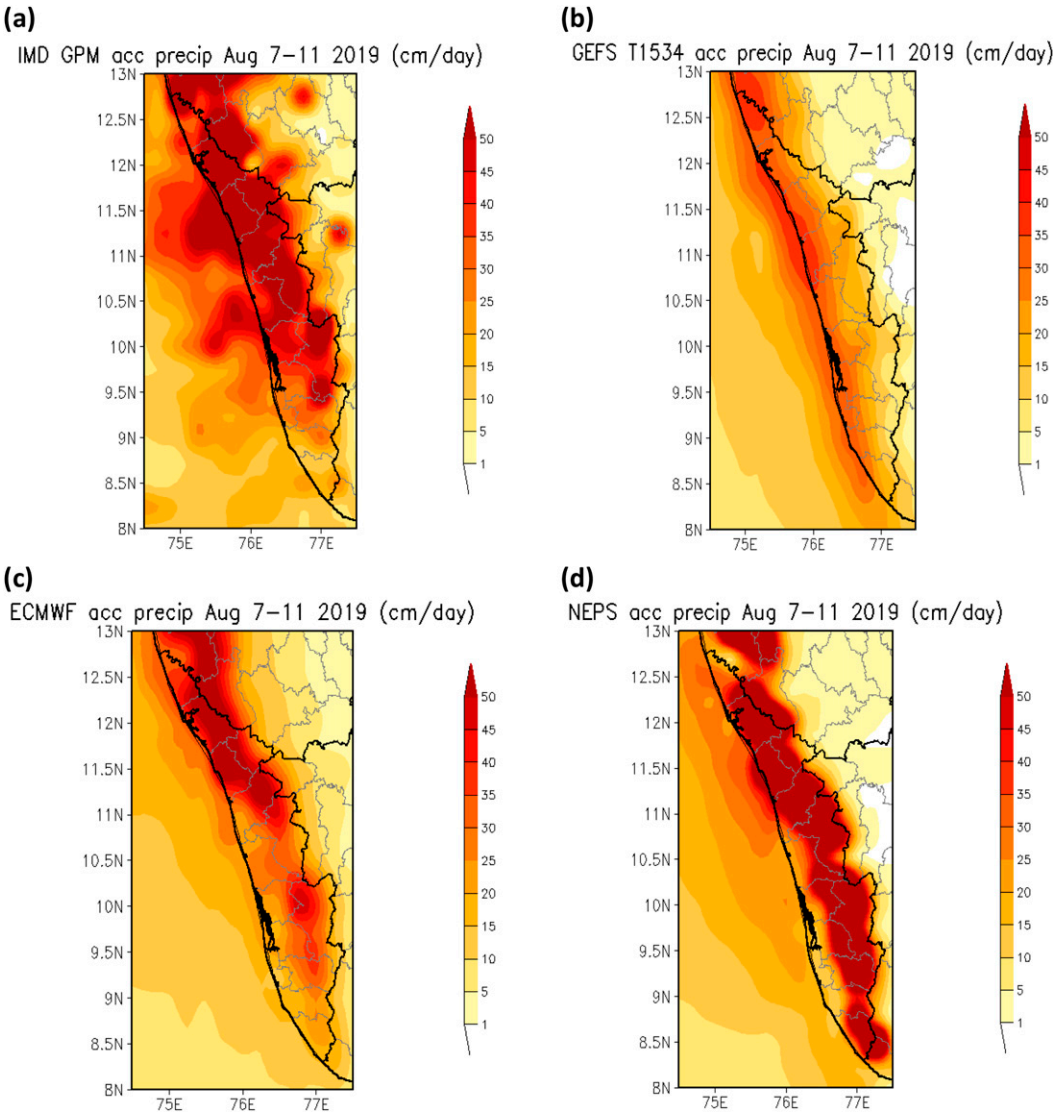

FIG. 14. As in Fig. 14, but for 7–11 Aug 2019 with forecast start time and date at 0000 UTC 6 Aug 2019.

predictive skill of the ensemble systems reduces to around 3 days with the NEPS showing a second peak in prediction skill beyond day 3 (second column in Fig. 15). Finally, increasing the precipitation threshold to three SD the predictive skill of the ensemble systems reduces to 1–2 days.

The above analysis has been repeated for the 7–11 August 2019 event and is displayed in Fig. 16. Now all models exhibit considerable skill, predicting the two SD rainfall anomalies up to day 5 with a probability of 90%, with the IFS and NEPS being able to predict reliably even the three SD anomalies beyond day 5.

The analyses of probabilistic forecast with different thresholds clearly showed that for extreme rainfall events with respect to climatology probabilistic forecast do extend the prediction horizon by several days compared to the high-resolution deterministic forecasts. In addition to the ensemble rainfall forecasts, the root-mean-square and anomaly correlation of 850-hPa wind fields and 500-hPa geopotential are found to be of higher skill for the ensemble models as compared to the deterministic forecasts (Table S1 in the online supplemental material). These analyses evidently suggest the high potential of ensemble forecast system during the extreme precipitation events of Kerala during August 2018 and 2019.

8. Conclusions

We have conducted an extensive study on the characterization and predictions of two exceptional rain events that occurred in the southern Indian state of Kerala during August 2018 and 2019.

First, we have used additional convection observations such as infrared satellite imagery, lightning data and radar reflectivities to demonstrate that the heavy rainfall events are largely

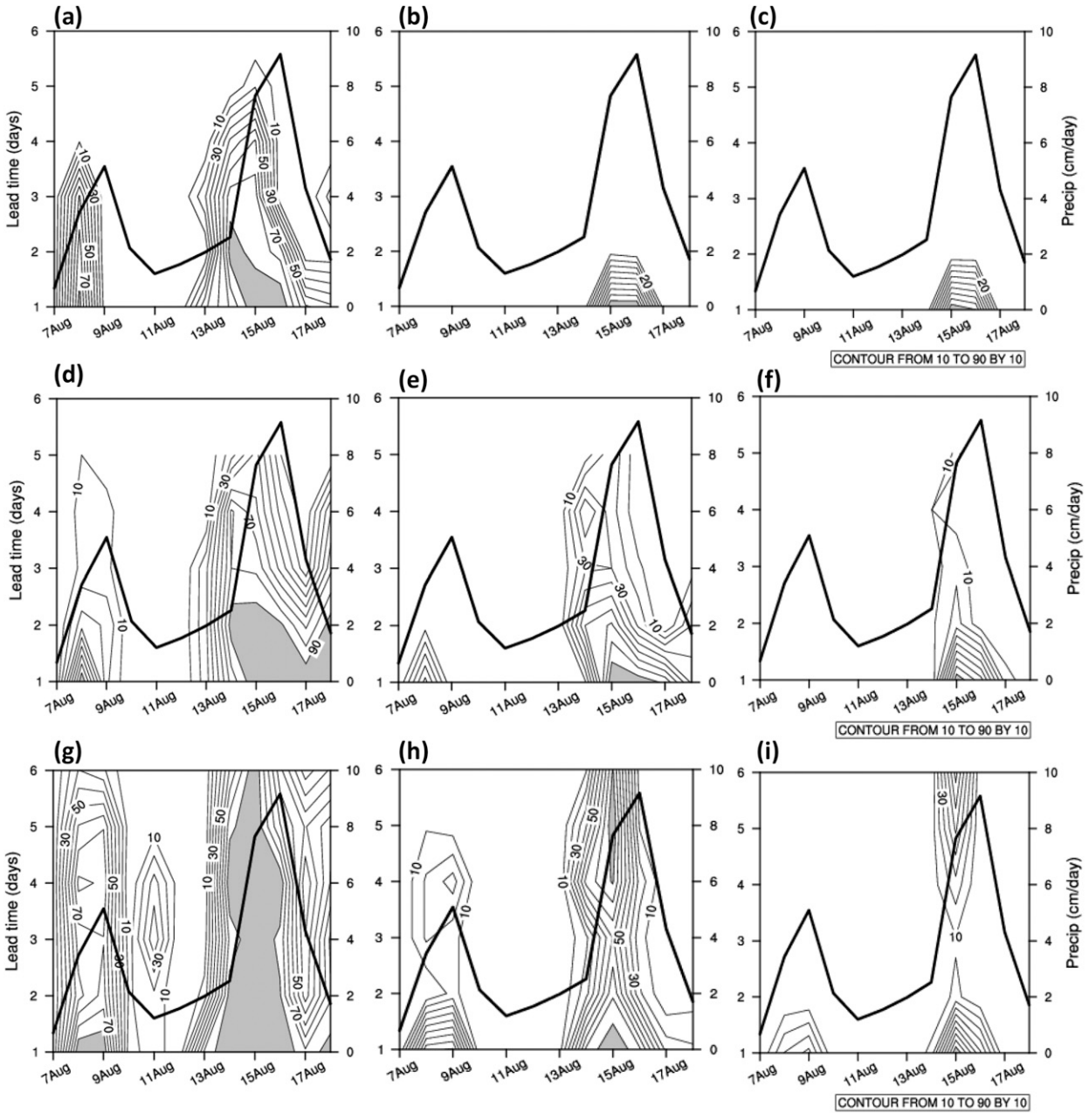

FIG. 15. Forecast lead time diagram of the probability (%) from (a)–(c) GEFS, (d)–(f) ECMWF, and (g)–(i) NCUM forecasts for the daily accumulated rain over Kerala (9.5°–11.5°N, 76°–77.5°E) exceeding the observed daily climatology (left) plus one standard deviation (SD), (center) two SD, and (right) three SD. The thick black line represents the IMD-GPM rainfall (cm day^{-1}) averaged for the same region for the period 6–19 Aug 2018. The gray shading represents probability > 90%.

associated with cumulus congestus and shallow convective clouds and associated orographic enhancement over the Ghats mountains. Deep convection also contributed to the 2019 event, but was not persistent.

A moisture budget analysis was then conducted using the ERA5 and three different global forecasting systems. The results showed that while strong moisture convergence is present in the 1000–800-hPa layer, the total column water tendency remained small, indicating a balance between moisture convergence and drying by precipitation. Interestingly, the evolution of area integrated moisture convergence with forecast lead time was consistent with the evolution of precipitation in the models, e.g., decreasing convergence with forecast lead time led to less precipitation and vice versa.

To characterize the large-scale forcing responsible for the strong moisture advection and convergence during the main

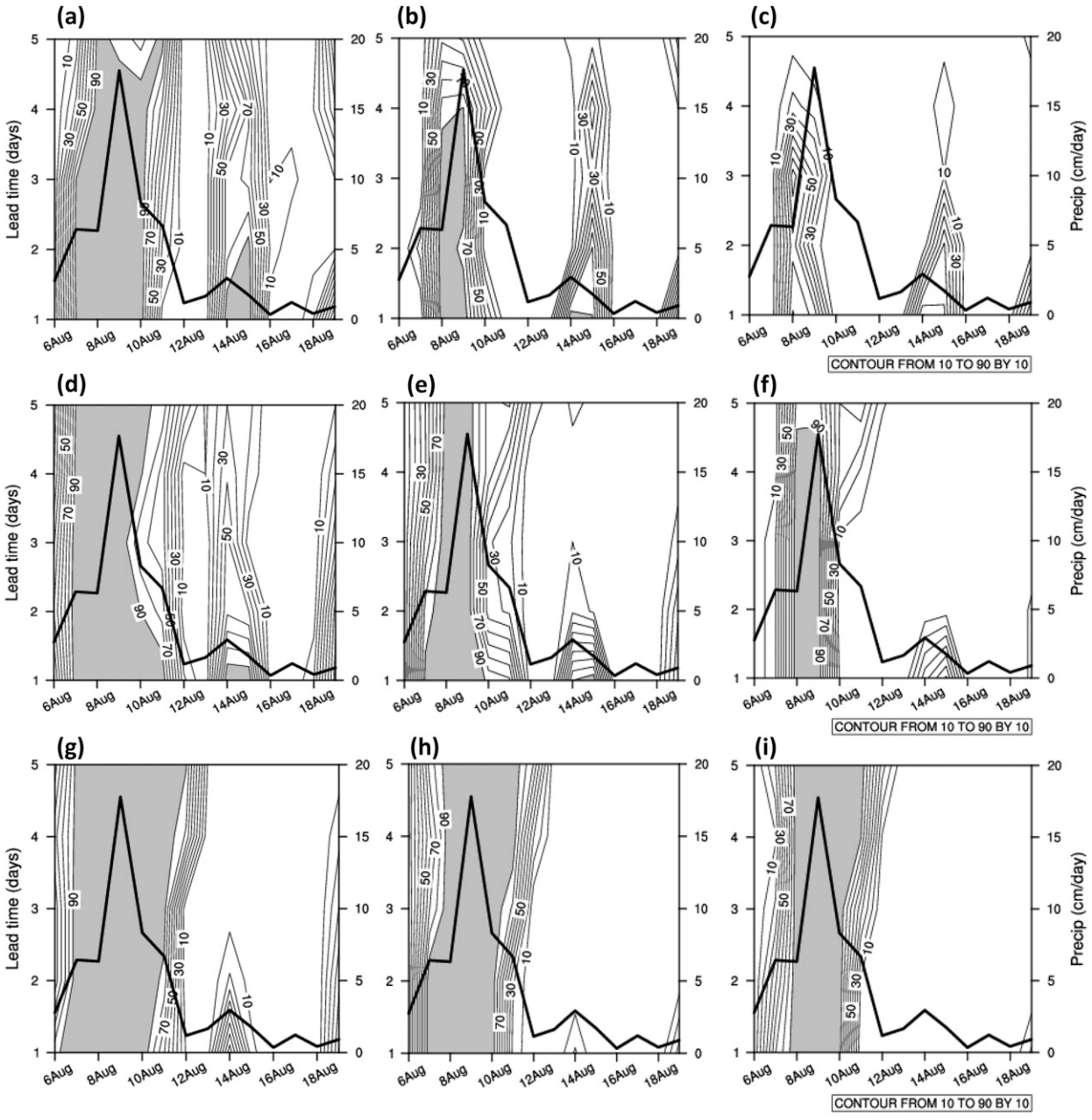

FIG. 16. As in Fig. 15, but for the period 6–19 Aug 2019.

rain episodes, a Rossby wave filter has been applied to the observed and predicted rainfall. We demonstrated that a high amplitude Rossby wave was in phase with the high moisture convergence and has actually led to the extreme rainfall. In addition, no excessive rainfall occurred on days, when the moisture convergence or the Rossby wave amplitude were high, but out of phase.

Furthermore, it is shown that the rainfall over Kerala is associated with the passage of westward-propagating Rossby waves, originating near 80°E for the 2018 event and near 90°E for the 2019 event. The forecast models clearly showed more robust and skillful forecasts of the 2019 Rossby waves beyond day-3 forecast range and were also more skillful in predicting the 2019 rain event compared to 2018.

Finally, a detailed evaluation of the three high-resolution deterministic and ensemble prediction systems was performed against a gridded rainfall dataset. Systematic differences between the models became apparent with large differences over the coastal mountains, with some models locating the main rainfall near the coast instead of further inland as observed. Generally, the ensemble predictions were more skillful than the deterministic forecasts, as they were able to predict rainfall

anomalies of more than three standard deviations from climatology beyond day 5 for August 2019 and up to day 3 for August 2018. In contrast, for these extreme events the deterministic forecasts appeared to be skillful roughly up to day 2 with a tendency of decreasing the precipitation amount with forecast lead time. The strong Rossby wave forcing in 2019 lead to overall more predictive skill in the models, underlining that predicting large-scale tropical wave forcing is key for skillful longer-range predictions of tropical rainfall anomalies.

Acknowledgments. IITM is fully funded by Ministry of Earth Sciences (MoES), government of India. The GEFS/GFS, NEPS/NCUM model run and analyses are being done in MoES High Power Computer (HPC) System at IITM, Pune, and NCMRWF, Noida, India, respectively. Director, IITM, Pune, is gratefully acknowledged for encouragement of the study. The authors would like to thank ECMWF for providing the ERA5 dataset (https://www.ecmwf.int/en/forecasts/datasets/reanalysis-datasets/era5). Further, the authors sincerely thank IMD for providing the IMD-GPM merged data, long-term gridded rainfall data, ground-based rain gauge data, and radar data. Cochin University of Science and Technology, Kochi, Kerala, India, is thankfully acknowledged for the wind profiler data. ISRO's Meteorological and Oceanographic Satellite Data Archival Centre (http://mosdac.gov.in) is duly acknowledged for providing brightness temperature data. The director at IITM is thanked for allowing us to use IITM-IAF ground-based lightening data. Finally, AS acknowledges the funding support from National Monsoon Mission program of MoES-IITM.

REFERENCES

Balsamo, G., P. Viterbo, A. Beljaars, B. van den Hurk, M. Hirschi, A. K. Betts, and K. Scipal, 2009: A revised hydrology for the ECMWF model: Verification from field site to terrestrial water storage and impact in the integrated forecast system. *J. Hydro. Meteor.*, **10**, 623–643, https://doi.org/10.1175/2008JHM1068.1.

Bechtold, P., N. Semane, P. Lopez, J. Chaboureau, A. Beljaars, and N. Bormann, 2014: Representing equilibrium and nonequilibrium convection in large-scale models. *J. Atmos. Sci.*, **71**, 734–753, https://doi.org/10.1175/JAS-D-13-0163.1.

Bellouin, N., J. Rae, A. Jones, C. Johnson, J. Haywood, and O. Boucher, 2011: Aerosol forcing in the Climate Model Intercomparison Project (CMIP5) simulations by HadGEM2-ES and the role of ammonium nitrate. *J. Geophys. Res.*, **116**, D20206, https://doi.org/10.1029/2011JD016074.

Best, M. J., and Coauthors, 2011: The Joint UK Land Environment Simulator (JULES), model description—Part 1: Energy and water fluxes. *Geosci. Model Dev.*, **4**, 677–699, https://doi.org/10.5194/gmd-4-677-2011.

Bowler, N. E., A. Arribas, S. E. Beare, K. R. Mylne, and G. J. Shutts, 2009: The local ETKF and SKEB: Upgrades to the MOGREPS short-range ensemble prediction system. *Quart. J. Roy. Meteor. Soc.*, **135**, 767–776, https://doi.org/10.1002/qj.394.

Buehner, M., J. Morneau, and C. Charette, 2013: Four-dimensional ensemble-variational data assimilation for global deterministic weather prediction. *Nonlinear Processes Geophys.*, **20**, 669–682, https://doi.org/10.5194/npg-20-669-2013.

Coumou, D., and S. Rahmstorf, 2012: A decade of weather extremes. *Nat. Climate Change*, **2**, 491–496, https://doi.org/10.1038/nclimate1452.

Dube, A., R. Ashrit, A. Ashish, K. Sharma, G. R. Iyengar, E. N. Rajagopal, and S. Basu, 2014: Forecasting the heavy rainfall during Himalayan flooding—June 2013. *Wea. Climate Extremes*, **4**, 22–34, https://doi.org/10.1016/j.wace.2014.03.004.

Duchon, C. E., 1979: Lanczos filtering in one and two dimensions. *J. Appl. Meteor.*, **18**, 1016–1022, https://doi.org/10.1175/1520-0450(1979)018<1016:LFIOAT>2.0.CO;2.

Edwards, J. M., and A. Slingo, 1996: Studies with a flexible new radiation code. I: Choosing a configuration for a large-scale model. *Quart. J. Roy. Meteor. Soc.*, **122**, 689–719, https://doi.org/10.1002/qj.49712253107.

——, J. Manners, J. C. Thelen, W. J. Ingram, and P. G. Hill, 2018: The radiation code. Unified model documentation paper 23, Met Office, United Kingdom, 55 pp.

Ek, M. B., K. E. Mitchell, Y. Lin, E. Rogers, P. Grunmann, V. Koren, G. Gayno, and J. D. Tarpley, 2003: Implementation of Noah land surface model advances in the National Centers for Environmental Prediction operational mesoscale Eta model. *J. Geophys. Res.*, **108**, 8851, https://doi.org/10.1029/2002JD003296.

Forbes, R. M., A. M. Tompkins, and A. Untch, 2011: A new prognostic bulk microphysics scheme for the IFS. ECMWF Tech. Memo. 649, 30 pp., https://doi.org/10.21957/bf6vjvxk.

Gregory, D., and P. R. Rowntree, 1990: A mass flux convection scheme with representation of cloud ensemble characteristics and stability dependent closure. *Mon. Wea. Rev.*, **118**, 1483–1506, https://doi.org/10.1175/1520-0493(1990)118<1483:AMFCSW>2.0.CO;2.

Han, J., and H. Pan, 2011: Revision of convection and vertical diffusion schemes in the NCEP Global Forecast System. *Wea. Forecasting*, **26**, 520–533, https://doi.org/10.1175/WAF-D-10-05038.1.

——, M. L. Witek, J. Teixeira, R. Sun, H.-L. Pan, J. K. Fletcher, and C. S. Bretherton, 2016: Implementation in the NCEP GFS of a hybrid eddy-diffusivity mass-flux (EDMF) boundary layer parameterization with dissipative heating and modified stable boundary layer mixing. *Wea. Forecasting*, **31**, 341–352, https://doi.org/10.1175/WAF-D-15-0053.1.

——, W. Wang, Y. C. Kwon, S.-Y. Hong, V. Tallapragada, and F. Yang, 2017: Updates in the NCEP GFS cumulus convection schemes with scale and aerosol awareness. *Wea. Forecasting*, **32**, 2005–2017, https://doi.org/10.1175/WAF-D-17-0046.1.

Joseph, S., and Coauthors, 2015: North Indian heavy rainfall event during June 2013: Diagnostics and extended range prediction. *Climate Dyn.*, **44**, 2049–2065, https://doi.org/10.1007/s00382-014-2291-5.

Kavčič, I., and J. Thuburn, 2018: A Lagrangian vertical coordinate version of the ENDGame dynamical core. Part I: Formulation, remapping strategies, and robustness. *Quart. J. Roy. Meteor. Soc.*, **144**, 1649–1666, https://doi.org/10.1002/qj.3368.

Kleist, D. T., 2012: An evaluation of hybrid variational-ensemble data assimilation for the NCEP GFS. Ph.D. thesis, Dept. of Atmospheric and Oceanic Science, University of Maryland, College Park, 149 pp.

——, and K. Ide, 2015: An OSSE-based evaluation of hybrid variational–ensemble data assimilation for the NCEP GFS. Part II: 4DEnVar and hybrid variants. *Mon. Wea. Rev.*, **143**, 452–470, https://doi.org/10.1175/MWR-D-13-00350.1.

Kornhuber, K., and Coauthors, 2019: Extreme weather events in early summer 2018 connected by a recurrent hemispheric wave-7 pattern. *Environ. Res. Lett.*, **14**, 054002, https://doi.org/10.1088/1748-9326/ab13bf.

Kumar, S., A. Hazra, and B. N. Goswami, 2014: Role of interaction between dynamics, thermodynamics and cloud microphysics

on summer monsoon precipitating clouds over the Myanmar Coast and the Western Ghats. *Climate Dyn.*, **43**, 911–924, https://doi.org/10.1007/s00382-013-1909-3.

——, and Coauthors, 2018: Implementation of new high resolution NCUM analysis-forecast system in Mihir HPCS. NCMRWF, NMRF/TR/01/2018, 21 pp., http://www.ncmrwf.gov.in/NCUM-Report-Aug2018_final.pdf.

Lock, A., A. Brown, M. Bush, G. Martin, and R. Smith, 2000: A new boundary layer mixing scheme. Part I: Scheme description and single-column model tests. *Mon. Wea. Rev.*, **128**, 3187–3199, https://doi.org/10.1175/1520-0493(2000)128<3187:ANBLMS>2.0.CO;2.

Lott, F., and M. J. Miller, 1997: A new subgrid-scale orographic drag parametrization: Its formulation and testing. *Quart. J. Roy. Meteor. Soc.*, **123**, 101–127, https://doi.org/10.1002/qj.49712353704.

Maheskumar, R. S., and Coauthors, 2014: Mechanism of high rainfall over the Indian west coast region during the monsoon season. *Climate Dyn.*, **43**, 1513–1529, https://doi.org/10.1007/s00382-013-1972-9.

Mamgain, A., A. Sarkar, A. Dube, T. Arulalan, P. Chakraborty, J. P. George, and E. N. Rajagopal, 2018: Implementation of very high resolution (12 km) global ensemble prediction system at NCMRWF and its initial validation. NCMRWF, NMRF/TR/02/2018, 25 pp., http://www.ncmrwf.gov.in/NEPS_TR_Aug2018_Final.pdf.

Mishra, S. K., S. Sahany, P. Salunke, I.-S. Kang, and S. Jain, 2018: Fidelity of CMIP5 multi-model mean in assessing Indian monsoon simulations. *Climate Atmos. Sci.*, **1**, 39, https://doi.org/10.1038/s41612-018-0049-1.

Mitra, A. K., A. K. Bohra, M. N. Rajeevan, and T. N. Krishnamurti, 2009: Daily Indian precipitation analyses formed from a merged of rain-gauge with TRMM TMPA satellite derived rainfall estimates. *J. Meteor. Soc. Japan*, **87A**, 265–279, https://doi.org/10.2151/jmsj.87A.265.

Mlawer, E. J., S. J. Taubman, P. D. Brown, M. J. Iacono, and S. A. Clough, 1997: Radiative transfer for inhomogeneous atmospheres: RRTM, a validated correlated-k model for the longwave. *J. Geophys. Res.*, **102**, 16 663–16 682, https://doi.org/10.1029/97JD00237.

Pattanaik, D. R., D. S. Pai, and B. Mukhopadhyay, 2015: Rapid northward progress of monsoon over India and associated heavy rainfall over Uttarakhand: A diagnostic study and real time extended range forecast. *Mausam*, **66**, 551–568.

Richardson, D. S., 2000: Skill and relative economic value of the ECMWF ensemble prediction system. *Quart. J. Roy. Meteor. Soc.*, **126**, 649–667, https://doi.org/10.1002/qj.49712656313.

Roca, R., M. Viollier, L. Picon, and M. Desbois, 2002: A multisatellite analysis of deep convection and its moist environment over the Indian Ocean during the winter monsoon. *J. Geophys. Res.*, **107**, 8012, https://doi.org/10.1029/2000JD000040.

Rotunno, R., and R. A. Houze, 2007: Lessons on orographic precipitation from the Mesoscale Alpine Programme. *Quart. J. Roy. Meteor. Soc.*, **133**, 811–830, https://doi.org/10.1002/qj.67.

Scaife, A. A., and Coauthors, 2017: Tropical rainfall, Rossby waves and regional winter climate predictions. *Quart. J. Roy. Meteor. Soc.*, **143**, 1–11, https://doi.org/10.1002/qj.2910.

Screen, J. A., and I. Simmonds, 2014: Amplified mid-latitude planetary waves favour particular regional weather extremes. *Nat. Climate Change*, **4**, 704–709, https://doi.org/10.1038/nclimate2271.

Shashikanth, K., K. Salvi, S. Ghosh, and K. Rajendran, 2014: Do CMIP5 simulations of Indian summer monsoon rainfall differ from those of CMIP3? *Atmos. Sci. Lett.*, **15**, 79–85, https://doi.org/10.1002/asl2.466.

Shige, S., and C. D. Kummerow, 2016: Precipitation-top heights of heavy orographic rainfall in the Asian monsoon region. *J. Atmos. Sci.*, **73**, 3009–3024, https://doi.org/10.1175/JAS-D-15-0271.1.

Smith, R. N. B., 1990: A scheme for predicting layer clouds and their water contents in a general circulation model. *Quart. J. Roy. Meteor. Soc.*, **116**, 435–460, https://doi.org/10.1002/qj.49711649210.

Soichi, S., and C. D. Kummerow, 2016: Precipitation-Top Heights of Heavy Orographic Rainfall in the Asian Monsoon Region. *J. Atmos. Sci.*, **73**, 3009–3024, https://doi.org/10.1175/JAS-D-15-0271.1.

Tennant, W. J., and S. Beare, 2014: New schemes to perturb sea-surface temperature and soil moisture content in MOGREPS. *Quart. J. Roy. Meteor. Soc.*, **140**, 1150–1160, https://doi.org/10.1002/qj.2202.

——, G. J. Shutts, A. Arribas, and S. A. Thompson, 2011: Using a stochastic kinetic energy backscatter scheme to improve MOGREPS probabilistic forecast skill. *Mon. Wea. Rev.*, **139**, 1190–1206, https://doi.org/10.1175/2010MWR3430.1.

Utsav, B., S. M. Deshpande, S. K. Das, and G. Pandithurai, 2017: Statistical characteristics of convective clouds over the Western Ghats derived from weather radar observations. *J. Geophys. Res. Atmos.*, **122**, 10 050–10 076, https://doi.org/10.1002/2016JD026183.

Vokoun, M., and M. Hanel, 2018: Comparing ALADIN-CZ and ALADIN-LAEF precipitation forecasts for hydrological modelling in the Czech Republic. *Adv. Meteor.*, **2018**, 5368438, https://doi.org/10.1155/2018/5368438.

Walters, D., and Coauthors, 2017: The Met Office Unified Model global atmosphere 6.0/6.1 and JULES global land 6.0/6.1 configurations. *Geosci. Model Dev.*, **10**, 1487–1520, https://doi.org/10.5194/gmd-10-1487-2017.

Webster, P. J., V. E. Toma, and H. M. Kim, 2011: Were the 2010 Pakistan floods predictable? *Geophys. Res. Lett.*, **38**, L04806, https://doi.org/10.1029/2010GL046346.

Wheeler, M., and G. N. Kiladis, 1999: Convectively coupled equatorial waves: Analysis of clouds and temperature in the wavenumber–frequency domain. *J. Atmos. Sci.*, **56**, 374–399, https://doi.org/10.1175/1520-0469(1999)056<0374:CCEWAO>2.0.CO;2.

Wilson, D. R., and D. P. Ballard, 1999: A microphysically based precipitation scheme for the UK Meteorological Office Unified Model. *Quart. J. Roy. Meteor. Soc.*, **125**, 1607–1636, https://doi.org/10.1002/qj.49712555707.

Yanai, M., S. Esbensen, and J. H. Chu, 1973: Determination of bulk properties of tropical cloud clusters from large-scale heat and moisture budgets. *J. Atmos. Sci.*, **30**, 611–627, https://doi.org/10.1175/1520-0469(1973)030<0611:DOBPOT>2.0.CO;2.

Zhao, P., Q. J. Wang, W. Wu, and Q. Yang, 2020: Which precipitation forecasts to use? Deterministic versus coarser-resolution ensemble NWP models. *Quart. J. Roy. Meteor. Soc.*, **147**, 900–913, https://doi.org/10.1002/qj.3952.

Zhao, Q., and F. H. Carr, 1997: A prognostic cloud scheme for operational NWP models. *Mon. Wea. Rev.*, **125**, 1931–1953, https://doi.org/10.1175/1520-0493(1997)125<1931:APCSFO>2.0.CO;2.

Zhou, X., Y. Zhu, D. Hou, and D. Kleist, 2016: A comparison of perturbations from an ensemble transform and an ensemble Kalman filter for the NCEP Global Ensemble Forecast System. *Wea. Forecasting*, **31**, 2057–2074, https://doi.org/10.1175/WAF-D-16-0109.1

——, ——, ——, Y. Luo, J. Peng, and D. Wobus, 2017: Performance of the new NCEP Global Ensemble Forecast System in a parallel experiment. *Wea. Forecasting*, **32**, 1989–2004, https://doi.org/10.1175/WAF-D-17-0023.1.